UNIVERSITÄTSKLINIKUM HAMBURG-EPPENDORF

Klinik und Poliklinik für Gefäßmedizin,
Universitäres Herz- und Gefäßzentrum

Prof. Dr. med. E. Sebastian Debus

Clamping of the infrarenal aorta results in intimal hyperplasia and distinct changes of S1P receptor expression in the intima-media and adventitia

Dissertation

zur Erlangung des Grades eines Doktors der Medizin /Zahnmedizin
an der Medizinischen Fakultät der Universität Hamburg.

vorgelegt von:

Yu Jiang

aus Jiangsu (China)

Hamburg 2021

Angenommen von der
Medizinischen Fakultät der Universität Hamburg am: 21.03.2022

Veröffentlicht mit Genehmigung der
Medizinischen Fakultät der Universität Hamburg.

Prüfungsausschuss, der Vorsitzende: Prof. Dr. Edzard Schwedhelm

Prüfungsausschuss, zweiter Gutachter: Prof. Dr. Axel Antonio Larena-Avellaneda

Table of contents

1. Introduction

1.1 Restenosis

Vascular obstruction may be treated by open surgery or interventional therapy. After successful revascularization, re-narrowing of the arteries occurs in a substantial number of patients. This phenomenon is called 'restenosis' and still is a major limitation in vascular medicine (Illuminati et al. 2017). The term 'restenosis' was originally used to describe recurrent heart valvular narrowing and was later extended to define recurrent vessel lumen narrowing (Stoney and String 1976).

The restenosis rates reported differ, especially depending on the modality of treatment, the vascular bed treated and study design (Lemson et al. 2000). Open surgical therapies generally produce less restenosis, although they are much more invasive. The rate of bypass occlusions due to restenosis also depends on the material implanted: venous femoro-crural bypasses show much better results than those with alloplastic prostheses (Ambler and Twine 2018).

Endoluminal vascular therapy was introduced by Dotter 1963 and remarkably improved by Grüntzig in 1974 (Barton et al. 2014). The widely introduced percutaneous transluminal angioplasty (PTA) using balloons in the 1980s increased the awareness of restenosis (Holmes et al. 1984) as clinical trials report high restenosis rates after PTA treatment in various arteries, e.g., up to 53% in coronary arteries, up to 62% in peripheral arteries and up to 100% in renal arteries (Table 1). This situation has been greatly improved by the introduction of endovascular stents (Puel et al. 1988) that significantly reduced restenosis rates (Table 1). A further reduction of restenosis rates after PTA was achieved by the introduction of drug eluting stents (DES) (Moses et al.

2003) (Table 1), specifically in coronary arteries. while the benefit in peripheral arteries was smaller (Colombo et al. 2003) (Table 1).

Still, restenosis plays a significant role after cardiovascular intervention. After stent angioplasty, there are 3 mechanisms that lead to lumen narrowing elastic recoil, vessel remodeling and intimal hyperplasia (IH).

Elastic recoil usually occurs between a few seconds up to minutes after endovascular angioplasty. It is the result of elastic laminae contraction and mainly occurs after balloon deflation (Buccheri et al. 2016). Negative vessel remodeling after stent angioplasty refers to lumen narrowing by constrictive reorganization of the vessel wall similar to wound healing (Buccheri et al. 2016).

IH remains as the main cause for both in-stent restenosis and the narrowing that can be observed after open vascular operations (Weintraub 2007).

Thus, further studying the mechanisms of IH, may lead to the development of novel pharmacological treatments to prevent restenosis as well as the identification of biomarkers of restenosis to tailor the patient's therapy.

Table 1. Representative restenosis rates (in percent) by location and intervention (at follow-up of 1-24 months)

Location	Procedure	Restenosis (%)	Follow-up	Reference
Coronary	PTA	21-53 (mean 40)	9 months	(Moses et al. 2003)
Coronary	Stent	16-44 (mean 25)	9 months	(Moses et al. 2003)
Coronary	Atherectomy	27-39	1 year	(Bittl et al. 2004)
Coronary	DES	0-16	2 years	(Moses et al. 2003)
Renal	PTA	27-100	6 months	(Leertouwer et al. 2000)
Renal	Stent	0-39 (mean 17)	12 months	(Leertouwer et al. 2000)
Iliac	PTA	22-34	1 year	(Dormandy et al. 2000)
Iliac	Stent	10-26	1 year	(Dormandy et al. 2000)
Femoral popliteal	PTA	39-62	1 year	(Dormandy et al. 2000)
Femoral popliteal	Stent	34-47	1 year	(Becquemin et al. 2003)
Femoral popliteal	DES	44	2 years	(Becquemin et al. 2003)
Carotid	Endarterectomy	1.7-9.3	2 years	(Katras et al. 2001)
Carotid	Stent	2.7-21	18 months	(Lal et al. 2003)

The restenosis rates show a wide variation depending on different study designs, vessel locations and intervention methods. Percutaneous Transluminal Angioplasty (PTA) has been widely adopted in the 1980s, when it was applied to various arteries. However, it caused the highest restenosis rates of all interventions. In the 1970s, for instance, PTA treatment in renal artery was followed by up to 100% re-occlusions between 6 and 12 months. The introduction of stents presented a breakthrough to decrease restenosis rates. Stents (bare metal stents) reduce restenosis rates after percutaneous coronary intervention (PCI) from 40% to 25% in average within 2 years. Another breakthrough has been achieved by the introduction of drug-eluting stents (DES) which further decreased coronary artery restenosis rates. DES, however, were not able to reduce restenosis rates in the femoro-popliteal artery compared to bare metal stents.

1.2 The role of vascular smooth muscle cells in IH

The blood vessel consists of three layers: the intima, media and adventitia, whereby the media is bordered by the internal and external elastic lamina (IEL, EEL), respectively (see Figure 1). The intima is composed of the endothelium, which has contact to the blood and subendothelial connective tissue. The media is mainly composed of vascular smooth muscle cells (VSMC), elastic fibers and extracellular matrix. The adventitia is the outer layer of vessels and consists of fibroblasts, progenitor cells, resident leukocytes and matrix including collagens (Figure 1) (Jennette and Stone 2014).
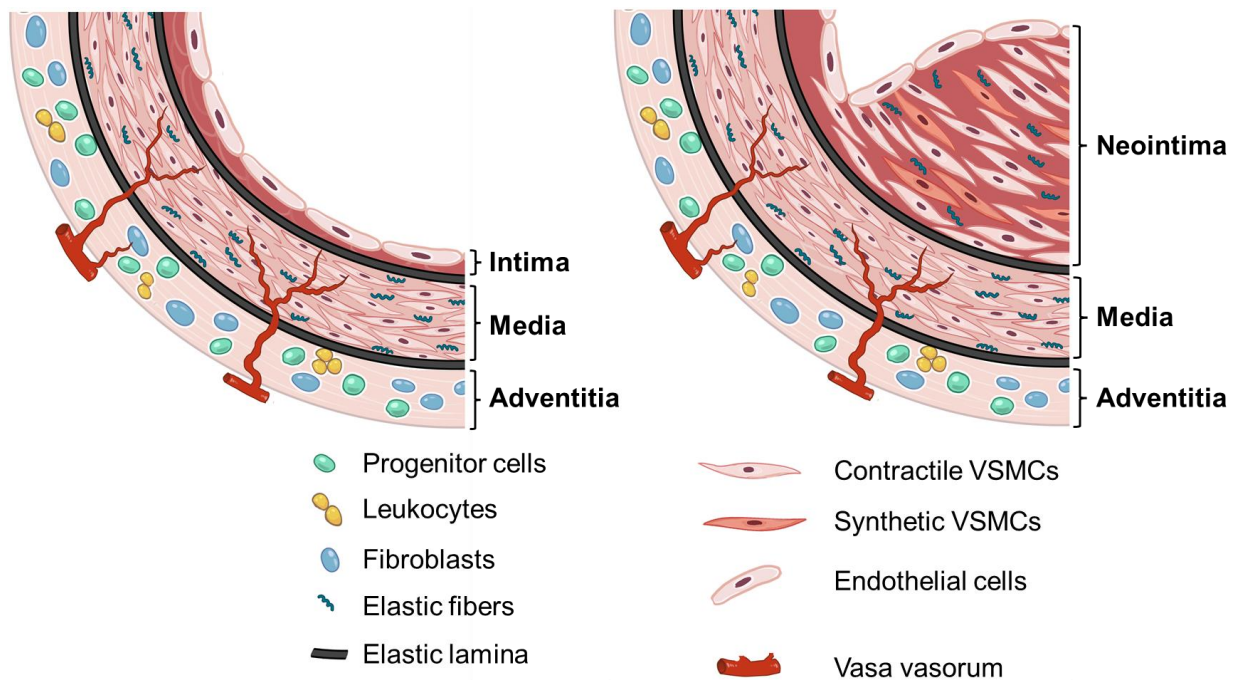
Figure 1. Anatomy of a vessel and IH. The fundamental structure of the artery is formed by three layers, intima, media and adventitia, which are divided by two elastic laminas. In rodents, the intima exclusively consists of endothelial cells whereas human arteries often present with subendothelial intimal cells. The media is bordered by the internal and the external elastic lamina. It consists of vascular smooth muscle cells embedded between elastic fibers and collagens. The adventitia is a layer with various cell types located between the external elastic lamina and the surrounding tissue. IH is a pathological process in which smooth muscle cells of the media migrate through internal elastic lamina into the intima where they proliferate and produce extracellular matrix to form a growing subendothelial layer. Authors own presentation.

IH is generally characterized by injury-induced proliferation and migration of arterial VSMCs into the intima, where they further contribute to lumen narrowing by producing extracellular matrix (Figure 1) (Jennette and Stone 2014). In homeostasis, VSMCs are largely quiescent. Vascular endothelial cells (ECs) play a role by producing inhibitors for VSMC proliferation and migration such as nitric oxide (NO) and prostacyclin. In agreement with this, loss of endothelial integrity has been shown to promote IH in small animal models including the balloon-injured rat carotid artery (Clowes et al. 1983). In this model, it has also been observed, that higher re-endothelialization rates are associated with reduced IH (Hayashi et al. 2000). VSMCs form the arterial media and their main function is to regulate the blood pressure by vessel contraction or dilation. In

the physiological state VSMCs are differentiated cells and exhibit a contractile phenotype characterized by a high expression of specific genes such as smooth muscle α-actin (SMA), smooth muscle myosin heavy chain 11 (MYH11) and smoothelin (Kraiss and Clowes 1997). The common transcriptional regulation of these genes relies on the CArGbox, a promoter element which is found in both 5' end and intronic regions. It is the binding domain of serum response factor (SRF) in combination with myocardin or a myocardin-related transcription factor (MRTF) as cofactor (McDonald et al. 2016, Owens et al. 2004). Upon arterial injury, VSMCs acquire a synthetic phenotype that is characterized by a loss of expression of SMC-specific genes and a gain of proliferative and migratory capacity as well as expression of matrix metalloproteinases (MMPs) and proteoglycans which play a role in matrix remodeling (Majesky 2016). The major mechanism underlying the injury-induced phenotypical change of VSMCs is the switch of the SRF cofactor from myocardin/MRTF to a ternary complex factor (TCF) of the Erythroblast Transformation Specific (ETS)-domain family such as Elk-1. Many SMC-specific genes contain TCF binding sites near adjacent CArG elements. Growth factors activate ERK-1/2 which phosphorylates TCFs such as Elk-1. Phosphorylated Elk-1 competes with myocardin for SRF binding thereby repressing the expression of SMC-specific genes and inducing growth promoting genes such as c-fos (Owens et al. 2004, Wang et al. 2004).

A role for medial VSMCs in IH has been proposed for decades now based on ultrastructural studies in which a rat infrarenal abdominal aorta denudation model was used and VSMCs in the neointima have been identified following electron microscopic analyses (Schwartz et al. 1975) and by the observation that medial VSMC proliferate upon balloon-injury of the rat carotid (Clowes et al. 1983). Nevertheless, when bone marrow-derived cells exhibiting some SMC-like properties such as SMA expression

have been detected in the circulation, a contribution of these cells to neointimal lesions after arterial injury has been intensively studied (Remy-Martin et al. 1999, Simper et al. 2002, Sata et al. 2002). Although using mice with green fluorescent protein (GFP)-labeled bone-marrow in various arterial injury models including wire injury, cuff replacement and carotid ligation, failed to demonstrate a substantial contribution of bone marrow-derived cells to neointimal lesions, a role for these cells in regulating IH cannot be excluded (Tanaka et al. 2003). Recent lineage tracing experiments using fluorescent labeling of VSMCs by MYH11-driven expression of Cre in ROSA mice confirm that VSMCs are the origin of neointimal cells after arterial injury (Nemenoff et al. 2011, Newman et al. 2018).

1.3. Is there a role for the adventitia in IH?

For decades, the adventitia was considered a connective tissue only to position vessels in their surroundings. Recent studies, however, support the idea that adventitial cells including fibroblasts, progenitor cells and inflammatory cells may regulate the response to vascular injury (Das et al. 2001). For instance, injury-induced proliferation and matrix production of adventitial cells has been shown to precede medial cell activation (Sartore et al. 2001, Dutzmann et al. 2017). Fibroblasts are the most abundant adventitial cells (Stenmark et al. 2013). After injury, they can transdifferentiate to myofibroblasts acquiring a SMC-like phenotype (Stenmark et al. 2013). Myofibroblasts are thought to be responsible for the negative remodeling of arteries following injury but their role in IH is unclear (Stenmark et al. 2013). Early work on balloon-injured porcine arteries showed that besides VSMCs, injury also induces proliferation of adventitial cells with remarkably higher rates for the latter (37% vs. 4%) (Shi et al. 1996).

Moreover, in the rat carotid artery, labeled adventitial fibroblasts have been detected in the neointima following balloon injury indicating that these cells migrated through the media (Li et al. 2000, Siow et al. 2003). A mouse vein graft model also provided evidence that adventitial cells contribute to neointimal formation: A mouse vena cava where the adventitia had been removed was planted into the position of the carotid artery of a recipient mouse and covered with adventitia from SM22-LacZ mouse. After 4 weeks, X-gal-stained tissue sections showed 30% of the neointimal VSMCs were from adventitial cells (Chen et al. 2013). These observations are consistent with data from a rat aortic-allograft model. Here, an abdominal aorta (AA) from a female F344 rat was taken and transplanted to replace the AA of a male LEW rat. The transplanted vessel was covered with isogenic adventitia tissue from a LEW rat that had been labeled with an orange fluorescent dye. This way, the authors found that 79% of the neointimal VSMCs were derived from the adventitia (Grudzinska et al. 2013).

In addition to fibroblasts and myofibroblasts, adventitial resident monocytes may also contribute to IH. Accumulation of the resident monocytes and macrophages in the adventitia is part of the early inflammatory response following arterial injury (Tang et al. 2008, Galkina et al. 2006). Consistent with a role for adventitial inflammation in IH is the finding that upon carotid ligation, Myd88-deficient mice show decreased accumulation of leukocytes in the adventitia and produce smaller intimal lesions when compared to wild-type animals (Tang et al. 2008). Taken together, these observations strongly suggest a role for adventitial cells in IH.

1.4 Mouse models for IH

Mouse models are widely used in biological and clinical research for several reasons. Mice are small, easily housed and handled. They have a fairly short lifespan and reproduce quickly. Most importantly, mouse genetics and biological characteristics resemble those of humans to an extent that many pathological conditions in humans can be modelled in mice.

Several mouse models have been established to study IH. Most common models include complete or partial flow reduction in carotid arteries or catheter-mediated removal of the endothelial layer (denudation) in carotid or femoral arteries.

Given the small size of these vessels, a serious limitation of these models is that many animals have to be used in order to obtain a sufficient amount of tissue to study medial and adventitial layers separately by biochemical or molecular biology methods. Therefore, models using bigger vessels like the aorta would be beneficial. Previously, it had been demonstrated that clamping of the abdominal mouse aorta results in endothelial denudation but it is unclear whether the clamped vessel responds with IH (Shirali et al. 2016). Here, we investigate whether aortic clamping produces neointimal lesions.

IH is a comprehensive response of the vessel wall involving many cell types and signaling pathways (Mills et al. 2012, Wamhoff et al. 2008). This work focuses on sphingosine-1-phosphate (S1P) and its receptors.

1.5 Sphingosine-1-phosphate (S1P) and S1P receptors (S1PRs)

S1P is a bioactive sphingolipid that plays a role in the regulation of many biological processes including leukocyte egress, endothelial barrier function, cancer, immunity

and cardiovascular functions. There are two pathways to synthesize S1P, a de novo pathway starting with a condensation reaction of serine and palmitoyl-CoA or by degradation of sphingomyelin (Figure 2). Both pathways generate ceramide and sphingosine as intermediates. By action of sphingosine-kinase type 1 or 2 (SphK1/2), sphingosine is phosphorylated to S1P. This process can be reversed by S1P phosphatases (SPPs) intracellularly or by lipid phosphate phosphatases (LPPs) at the cell surface. Also, S1P can be irreversibly cleaved by S1P-lyase (SPGL) to yield hexadecenal and phosphoethanolamine (Figure 2) (Winkler et al.2017). S1P is abundant in plasma where it is mainly bound to high density lipoproteins (HDL) via apolipoprotein M (ApoM) and albumin (Christoffersen et al. 2011). The sources of plasma S1P include red blood cells (RBCs), endothelial cells and platelets (Mendelson et al. 2014). S1P is produced intracellularly and then exported into the circulation by specific transporters including Spinster homolog 2 (SPNS2) in endothelial cells and major facilitator superfamily domain- containing protein 2B (MFSD2B) in RBCs (Fukuhara et al. 2012, Vu et al. 2017).
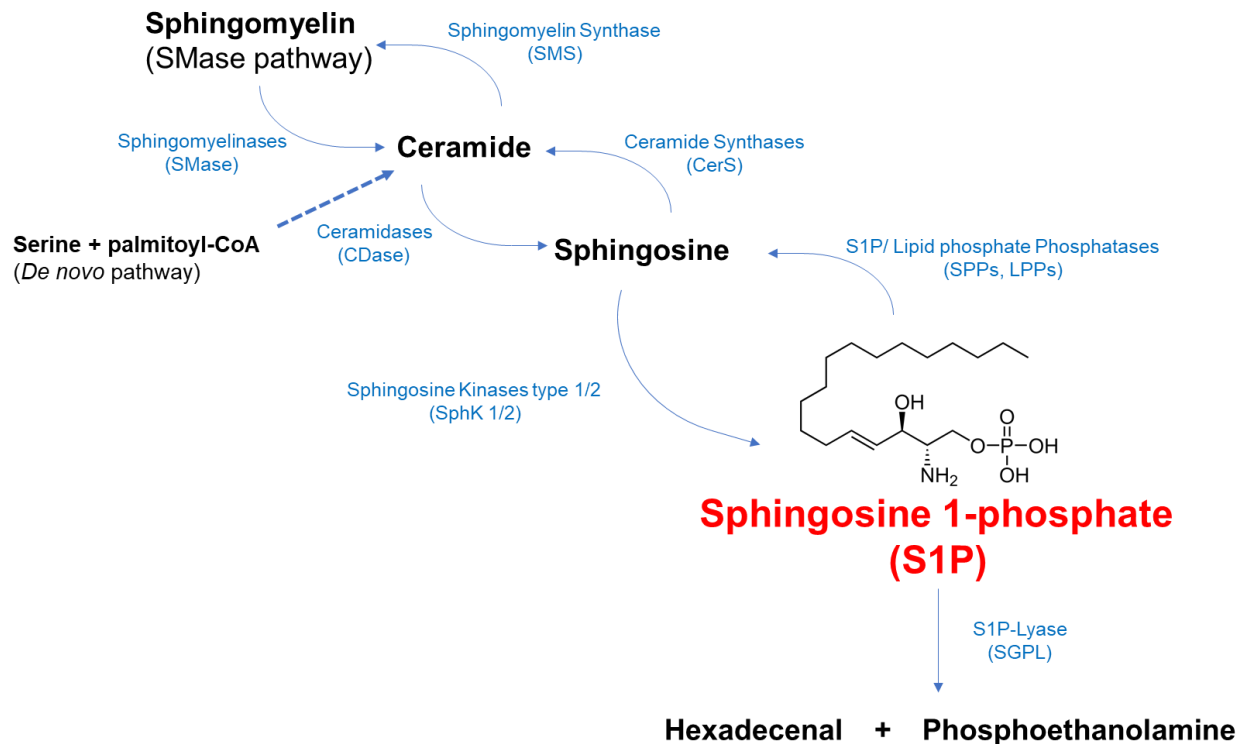
Figure 2. The metabolism of Sphingosine-1 phosphate (S1P). S1P can be synthesized in two ways: 1. by a de novo pathway starting with a condensation reaction of serine and palmitoyl-CoA and 2. by degradation of the membrane lipid sphingomyelin. Both pathways generate ceramide and sphingosine. Sphingosine kinases type 1 and 2 (SphK1 and SphK2) finally phosphorylate sphingosine to form S1P. This process can be reversed intracellularly by S1P phosphatases (SPPs) or at the cell surface by lipid phosphate phosphatases (LPPs). S1P can also be cleaved by S1P lyase (SGPL) into hexadecenal and phosphoethanolamine. (Modified from Winkler et al. 2017)

Biologic functions of S1P are mostly mediated by five specific, G-protein coupled receptors (S1PR1-5), whereby S1PR1-3 are ubiquitously expressed. S1PR1 exclusively couples to $G_{\alpha i}$ while S1PR2 and S1PR3 can couple to $G_{\alpha i}$, $G_{\alpha 12/13}$ as well as $G_{\alpha q}$ (Mendelson et al. 2014) (Figure 3). In arteries, S1PR1 is the main type of S1P receptor expressed in ECs, while VSMCs highly express S1PR2 and S1PR3 (Alewijnse et al. 2004). A more detailed expression pattern of S1P receptors including the adventitia has not been reported yet and is investigated in the present study.

S1PR1 S1PR2 S1PR3

$G_{\alpha i}$ $G_{\alpha 12/13}$ $G_{\alpha q}$

PI3K RhoA/ROCK PLC

Akt/eNOS ⊣ PTEN NF-κB SAPK IP3

Cell activity Ca^{2+}

Permeability

Inflammation
Coagulation

Constriction
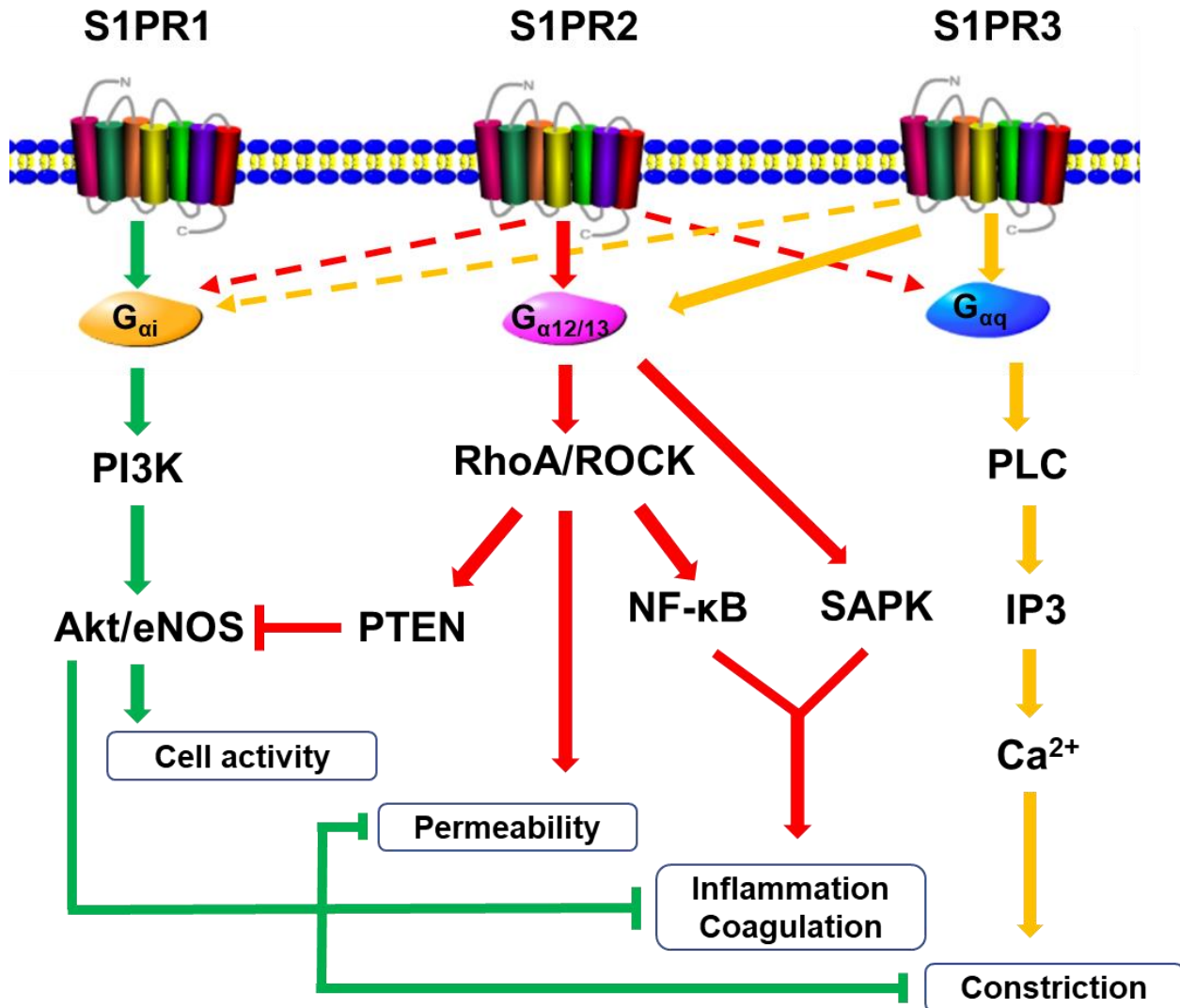
Figure 3. S1P receptor (S1PR1-3) signaling. S1P receptors couple to different G-proteins that activate different signaling pathways. In endothelial cells for instance, S1PR1 exclusively couples to $G_{\alpha i}$ while S1PR2 and S1PR3 can couple to $G_{\alpha i}$, $G_{\alpha 12/13}$ and $G_{\alpha q}$. S1PR1 is critical to maintain the endothelial barrier and attenuates inflammation in Phosphoinositid-3-kinase (PI3K)/Akt/eNOS-dependent way. Both S1PR2 and S1PR3 can couple to $G_{\alpha 12/13}$ activating Rho/ROACK which increases the vascular permeability. S1PR2 inhibits cell migration and proliferation via RhoA/ROCK-PTEN signaling and also promotes inflammation and coagulation via Rho/ROCK/NF-κB or SAPK p38 pathways. By coupling to $G_{\alpha q}$, S1PR3 promotes leukocyte rolling and P-selectin mobilization in a phospholipase C (PLC)/Ca^{2+}-dependent way. (Modified from Sanchez 2016)

1.5.1 S1PR1

The role of S1PR1 is essential in vascular development since genetically deleting

S1PR1 is embryonic lethal in mice due to severe bleeding caused by vasculature

immaturity (Liu et al. 2000). In endothelial cells, S1PR1 is critical to maintain the barrier

function. By activation of PI3K/Akt, and the small GTPases Rac1 and cell division control protein 42 homolog (Cdc42), S1PR1 signaling promotes the formation of adherens junction, tight junction assembly and cell-extracellular matrix adhesion, all strengthening cell-cell and cell-matrix interactions (Figure 3) (Xiong and Hla 2014, Morales-Ruiz et al. 2001). Endothelial S1PR1 also attenuates inflammation by inhibiting the expression of cell-adhesion molecules such as E-selectin, P-selectin and intercellular adhesion molecules-1 (ICAM-1) (Winkler et al. 2017).

As S1PR1 stimulates cell migration and proliferation via activating the PI3K/Akt pathway (Sanchez 2016), one may assume that S1PR1 expression promotes IH. Notably, S1PR1 appears to be higher expressed in VSMCs derived from FVB mice compared to C57BL/6 mice which may contribute to the observation that FVB mice form much larger lesions following carotid injury than C57BL/6 mice (Inoue et al. 2007, Hui 2008). Moreover, knocking down the expression of S1PR1 by Small interfering ribonucleic acid (siRNA) reduces migration in FVB VSMCs towards S1P (Inoue et al. 2007). Additional evidence supporting a lesion promoting role for S1PR1 following vascular injury came from a humanized rat model (Braetz et al. 2018). In this model, a human internal mammary artery (IMA) is implanted into the position of the abdominal aorta in an immune-suppressed rat. Only following a previous denudation of the IMA, transplanted vessels develop a significant neointima. Remarkably, not only are virtually all cells appearing in the intima S1PR1-positive at days 7 and 14 after surgery, but the number of S1PR1-positive cells also greatly increases in the media. Taken together, these observations suggest a role for S1PR1 in injury-induced proliferation and migration of VSMCs (Braetz et al. 2018).

1.5.2 S1PR2

S1PR2 may play an inhibitory role in IH since S1PR2 knock-out mice form significant larger lesions than their wild-type littermates after carotid ligation (Shimizu et al. 2007). In vascular cells, S1PR2 mainly couples to $G_{\alpha12/13}$ which mediates the activation of the small GTPase RhoA and its downstream effector Rho kinase (ROCK) (Figure 3) (Taha et al. 2004, Ikeda et al. 2003). In VSMCs, the activation of RhoA promotes stress fiber and focal adhesion formation which decreases VSMC migration (Ryu et al. 2002, Okamoto et al. 2000). In agreement with this, S1PR2 knock-out VSMCs do not activate RhoA in response to S1P stimulation and they also show increased migration in the presence of S1P (Shimizu et al. 2007).

In VSMCs, S1PR2-mediated RhoA activation also regulates the expression of VSMC differentiation genes (Grabski et al. 2009, Lockman et al. 2004). The activation of RhoA promotes the polymerization of G-actin into F-actin which releases cytosolic MRTF from G-actin. MRTF then enters the nucleus and forms a complex with SRF which then binds to CArG elements and stimulates the expression of VSMC differentiation genes (Wang et al. 2004, Wamhoff et al. 2008, Mack et al. 2001).

In ECs, the RhoA/ROCK pathway opposes the action of S1PR1 and increases vascular permeability (Figure 3). By RhoA/ROCK-dependent activation of the tyrosine phosphatase PTEN (Phosphatase and Tensin homolog), the PI3K/Akt signaling is decreased resulting in an inhibition of cell migration and survival (Sanchez 2016). GTP-bound $G_{\alpha12/13}$ also activates nuclear factor 'kappa-light-chain-enhancer' of activated B-cells (NF-κB) as well as the stress-activated protein kinase (SAPK) p38 thereby promoting inflammatory processes and coagulation (Figure 3) (Zhang et al. 2013, Lorenz et al. 2007)

1.5.3 S1PR3

In the vasculature, S1PR3 mainly couples to $G_{\alpha q}$ that regulates phospholipase C (PLC)/ inositol (1,4,5)-trisphosphate (IP3)-dependent calcium release from internal stores and VSMC contraction (Fukata et al. 2001). In agreement with this is the finding that the selective S1PR3 antagonist TY-52156 decreases intracellular Ca^{2+} concentration and inhibits cell constriction in human coronary artery smooth muscle cells (HCASMCs) (Murakami et al. 2010).

In ECs, S1PR3 regulates Akt-mediated phosphorylation of eNOS (endothelial nitric oxide synthase) resulting in enhanced nitric oxide (NO) production and vasodilation (Nofer et al. 2004, Tölle et al. 2016). Moreover, S1PR3 has been shown to promote leukocyte rolling and P-selectin mobilization via PLC/Ca^{2+}-dependent way and the recruitment of monocytes by coupling to $G_{\alpha q}$ (Figure 3) (Awojoodu et al. 2013, Nussbaum et al. 2015). Like S1PR2, S1PR3 can couple to $G_{\alpha 12/13}$ to increase vascular permeability in RhoA/ROCK-dependent way (Figure 3) (Lee et al. 1999).

The allover role of S1PR3 in IH is unclear as opposite effects have been reported depending on the injury model used. Carotid ligation in S1PR3 knock-out mice resulted in an increased neointima indicating an inhibitory role for S1PR3 in VSMC proliferation and migration (Keul et al. 2011). The opposite however, was found following femoral denudation. Here, S1PR3 knock-out mice produced smaller lesions than wild type animals (Shimizu et al. 2012). These apparently contradicting results may due to the different vascular beds (carotid vs. femoral artery) or the different mode of injury (ligation vs. denudation). When S1PR3 is introduced into VSMCs using a retroviral vector, cells gain migratory and proliferative capacity (Shimizu et al. 2012). It is therefore possible that S1PR3 expression in VSMCs promotes IH but that expression of S1PR3 in other cells type is inhibitory and depending on the vascular bed or the

mode of injury, one or the other effect prevails. To address this question, one objective of this work is to characterize S1PR3 expression in the media as well as in the adventitia using the abdominal denudation model.

1.6 Objectives of the study

This work has two main objectives. First, to establish a new mouse model for intima hyperplasia that involves clamping of the abdominal aorta. This vessel should be large enough to allow efficient separation of the adventitia and the intima-media (I-M) and should yield sufficient material for molecular examinations of these tissue layers by RT-qPCR without the need of using multiple animals per data point. Second, the expression of S1P receptors (S1PR1-3) as well as cell markers for VSMCs (MYH11), ECs (Cluster of differentiation 31 (CD31)), leukocytes (Cluster of differentiation 45 (CD45)) and monocytes/macrophages (Cluster of differentiation 68 (CD68)) will be measured by RT-qPCR to characterize the injury response and gain insight about the potential roles for S1P receptors in IH.

2. Methods and materials

2.1 Animal procedures

Mouse surgeries were performed in the animal facility of the University Hospital Hamburg-Eppendorf (UKE). C57BL/6 strain mouse was taken for surgeries. The animal work was approved by the local authorities (Behörde für Gesundheit und Verbraucherschutz, Freie und Hansestadt Hamburg; number of the proposal: N

043/2018). Surgeries were performed under a stereomicroscope (Leica, see Table 2) and all surgical instruments have been sterilized by autoclaving prior to use.

Table 2. The list of surgical instruments

Name	Catalog No.	Manufacturer
Spring scissor (straight)	No.15000-03	Fine Science Tools (F.S.T)
Fine Iris scissor (angled to side, 9 cm)	No.14063-09	Fine Science Tools (F.S.T)
Standard pattern surgical scissor (straight)	No.14001-12	Fine Science Tools (F.S.T)
Dumont #5 forceps (biology tip)	No.11295-10	Fine Science Tools (F.S.T)
Dumont #5/45 forceps	No.11251-35	Fine Science Tools (F.S.T)
Delicate Moria forceps (microserrated)	No.11370-32	Fine Science Tools (F.S.T)
Round handled suture tying forceps	No.18026-10	Fine Science Tools (F.S.T)
Round handled needle holder (straight with lock)	No.12075-12	Fine Science Tools (F.S.T)
Schwarz micro serrefines (strong pressure)	No.18052-03	Fine Science Tools (F.S.T)
Magnetic fixator retraction system:	No.18200-20	Fine Science Tools (F.S.T)
• Small base plate	No.18200-03	Fine Science Tools (F.S.T)
• Short fixator	No.18200-01	Fine Science Tools (F.S.T)
• Tall fixator	No.18200-02	Fine Science Tools (F.S.T)
• Elastomer (2 m roll)	No.18200-07	Fine Science Tools (F.S.T)
• Retractors (blunt, 1 mm wide)	No.18200-09	Fine Science Tools (F.S.T)
• Retractors (blunt, 2.5 mm wide)	No.18200-10	Fine Science Tools (F.S.T)
• Retractors (blunt, 5 mm wide)	No.18200-11	Fine Science Tools (F.S.T)
Cotton buds (non-sterile)	1260	Meditrade GmbH
Sterile compress	321075	Fink & Walter GmbH
ETHICON PERMA-HAND™ silk suture (7-0, black)	768G	Johnson & Johnson Medical Ltd
ETHICON ETHILON™ Polyamide 6 suture (10-0, black)	2814G	Johnson & Johnson Medical Ltd
ETHICON PROLENE™ Polypropylene suture (6-0, blue)	EH7406H	Johnson & Johnson Medical Ltd
BD Micro-Fine™ U-100 insulin syringes	324825	Becton Dickinson and Company
BD PLASTIPAK® sterile syringe (20 ml)	0050	Johnson & Johnson Medical Ltd
B. Braun Vasofix Safety Braunüle intravenous cannulas (G22, blue)	603034	ALMO-Erzeugnisse Erwin Busch GmbH
B. Braun Isis AESCULAP® battery-operated clipper	GT421	Aesculap Suhl GmbH
Leica stereomicroscope M60	10450167	Leica microsystems AG
Harvard apparatus anesthetic vaporizer	34-1040SV	Harvard Apparatus
Micro-Touch® medical examination gloves	700112	Ansell Limited
Microscope slide 76X26X1 mm	17590 219	Paul Marienfeld GmbH

2.1.1 Anesthesia and surgery preparation

The operating table was disinfected by wiping with 70% ethanol and a surgical pad placed onto it. The surgical heating platform (Fine Science Tools, see Table 2) was turned on and the assembled magnetic fixator retraction system (Fine Science Tools, see Table 2) and sterile saline were preheated to 37 °C (Figure 4A). Thirty minutes before surgery, mice were injected subcutaneously with a Buprenorphine/Rimadyl solution (12 µL/g) (Bayer Vital GmbH, Boehringer Ingelheim Vetmedica GmbH, see Table 3). Mice were then placed into the anesthesia induction chamber and given 4% isoflurane at a flow rate of 1 L/min (Figure 4B). Once the respiratory rate slowed, mice were placed onto a warming pad for surgical preparation. Isoflurane (1.5-2.0%) was administered from now on by using a face mask and adjusted, if necessary, to maintain adequacy of anesthesia (as evaluated by the toe pin test) as well as spontaneous respiration. Ophthalmic ointment was applied to the corneas, animals were placed supine and limbs were fixated by using sterile medical tape (Figure 4C). Hair was removed from the abdominal area by using clippers (Aesculap Suhl GmbH, see Table 2) and the surgical area disinfected by three alternating wipes with 0.1 g/ml Betaisodona (ACA Müller/ADAG Pharma AG, see Table 3) and 70% ethanol.
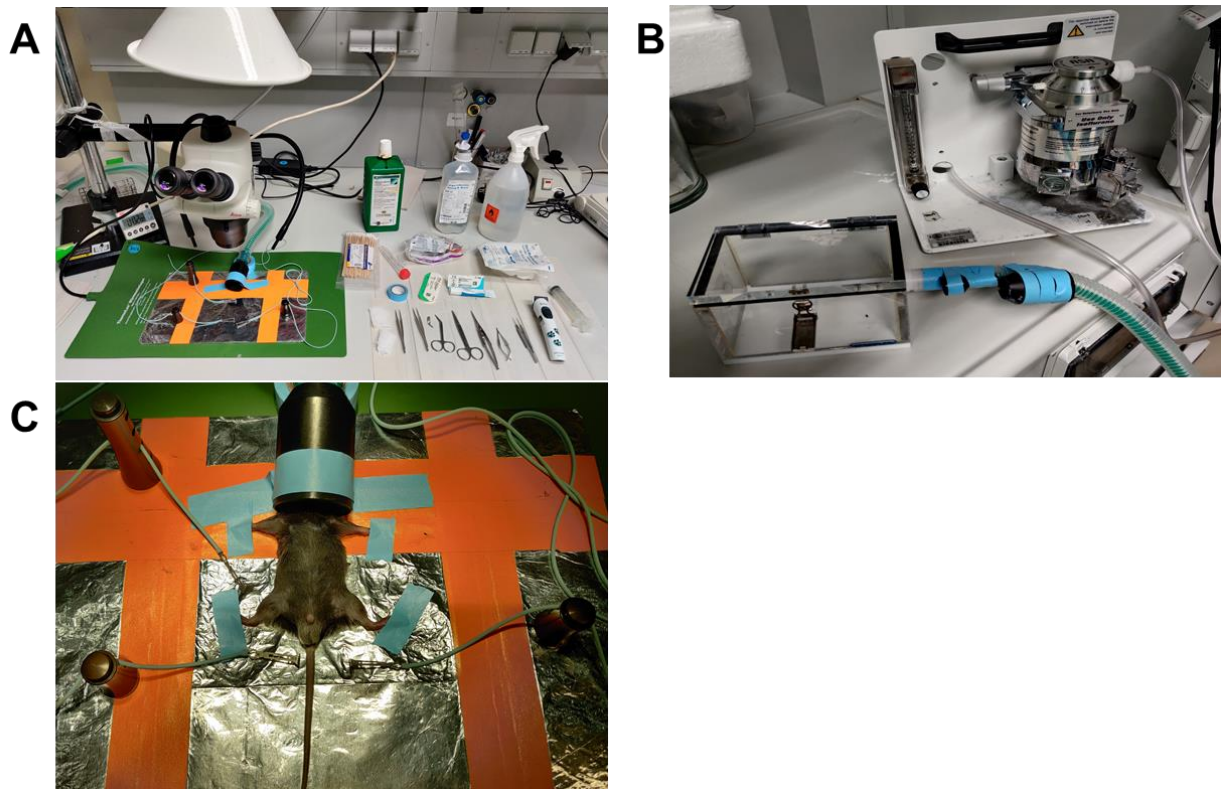
Figure 4. Surgery preparation and clamping procedure. Operating table and surgical instruments were disinfected and prepared **(A).** The anesthetic gas evaporator was filled with isoflurane and connected to oxygen and inducing chamber **(B)**. Mice were anesthetized and fixed with tapes **(C).**

2.1.2 Infrarenal aortic clamping

With a scalpel, a 2.5-3 cm long skin incision was made starting from the lower edge of the xiphoid process and following the midline of the abdomen. Using a magnetic retraction system, the skin was then carefully dissected by cutting away connective tissue with scissors. The abdominal cavity was opened by a 2-2.5 cm incision along the abdominal white line to avoid cutting muscle tissue. The exposed intestines were carefully lifted with saline-soaked cotton swabs onto a saline-soaked gauze placed proximal of the incision and then covered with another saline-soaked gauze. The rectum was lateralized by using a retractor to expose the base of the retroperitoneum from the inferior kidney pole to the bifurcation. The infrarenal aorta was then carefully dissected and separated from the vena cava. Aortic branches exposed during this

process were ligated with 10-0 ETHILON suture (Johnson & Johnson Medical Ltd, see Table 2). A 1.75 mm wide, strong pressure vascular clamp (Fine Science Tools, see Table 2, Figure 5A) was carefully placed just proximal of the bifurcation and the aorta clamped for 2 min (Figure 5B). The instrument was then moved proximally to clamp the adjacent section. In this way, 4 sections of the infrarenal aorta were clamped for 2 min each spanning the region between the bifurcation and close to the branch points of the renal arteries. These clamping steps were repeated 3 times so that each aortic section was occluded for 3 x 2 min. For each step, aortic occlusion was verified by the lack of pulsation distally of the clamp. If necessary, small bleedings were stopped by pressing cotton swabs against the wound. After clamping, intestines were finally carefully placed back into the abdominal cavity and rinsed with saline. The abdominal wall was closed by a continuous 6-0 absorbable suture (Johnson & Johnson Medical Ltd, see Table 2) followed by skin closure with a 6-0 silk mattress suture (Johnson & Johnson Medical Ltd, see Table 2). A sham operation group was included where mice underwent anesthesia and dissection of the infrarenal aorta without clamping before wound closure. The mice in the non-operated control group haven't undergone any surgical procedure.
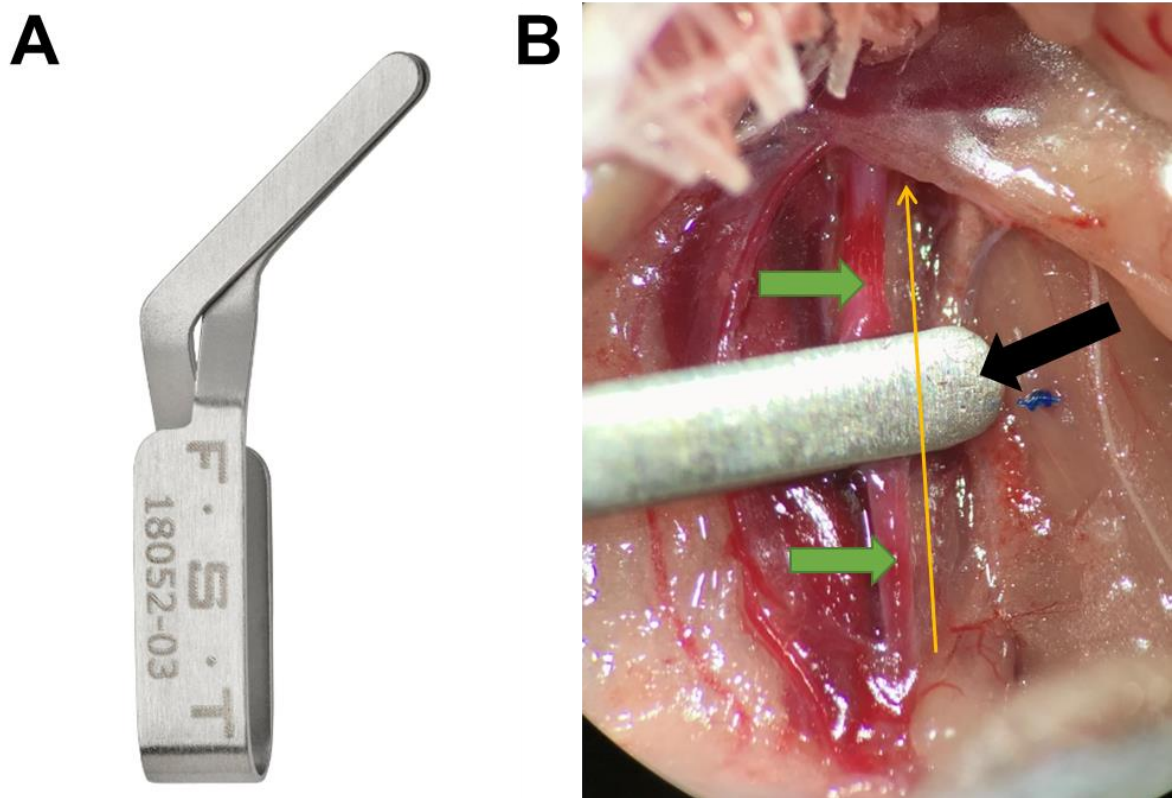
Figure 5. The clamping procedure on infrarenal abdominal aorta. After laparotomy and dissection of infrarenal abdominal aorta, the specific high-pressure vascular clamp was applied for injury **(A)**. The clamp was placed at proximal part of the bifurcation for 2 min and then moved proximally for 3 x 2 min until reached the branch points of the renal arteries. These clamping steps were repeated 3 times **(B)**. Green arrows: infrarenal abdominal aorta; black arrow: vascular clamp; orange arrow: the direction of clamping procedure.

2.1.3 Postoperative assessment and recovery

Following surgery, mice were placed onto a heating pad and monitored for any signs of respiratory distress until fully awake. After surgery, mice received Metamizole (200 mg/kg body weight) (Ratiopharm GmbH, see Table 3) in the drinking water for the following 7 days and Meloxicam (1 mg/kg body weight) (Ceva Tiergesundheit GmbH, see Table 3) in the food mash on the floor of the cage for the following 2 days. The wounds and the general health status of mice were assessed daily until sacrifice.

Table 3. The list of medications

Name	Manufacturer
Buprenovet® buprenorphine solution 0.3 mg/ml	Bayer Vital GmbH
Narcoren® Pentobarbital-sodium solution 16 g/100 ml	Boehringer Ingelheim Vetmedica GmbH
Rimadyl® Carprofen solution 50 g/20 ml	Pfizer GmbH
Baxter Isoflurane 250 ml	Baxter Deutschland GmbH
Ringer infusion solution	B.Braun Melsungen AG
Vidisic® eye gel carbomer 2 mg/g	Dr. Mann Pharma GmbH
Meloxidyl® Meloxicam oral suspension 0.5 mg/ml	Ceva Tiergesundheit GmbH
Novaminsulfon ratiopharm® Metamizole 500 mg/ml	Ratiopharm GmbH
Betaisodona solution 0.1g/ml	ACA Müller/ADAG Pharma AG

2.1.4 Sacrifice and tissue harvest

Mice were killed by intraperitoneal injection of an over-dose of pentobarbital (800 mg/kg body weight) (Boehringer Ingelheim Vetmedica GmbH, see Table 4) and fixed onto a preparation board using medical tape. The abdominal and thoracic cavities were opened, the heart exposed and a small hole was cut into the auricular dextra to allow perfusate outflow. A 22G infant scalp needle (ALMO-Erzeugnisse Erwin Busch GmbH, see Table 2) was inserted 3-4 mm into the left ventricle and 50 ml of ice-cold saline were slowly injected. When tissue was harvested for histological analysis, a perfusion with 30 ml of 4% formalin (Grimm med. Logistik GmbH, see Table 4) was performed subsequently and tissue transferred into 4% formalin (Grimm med. Logistik GmbH, see Table 4). Tissue harvested for RT-qPCR analysis was immediately transferred to RNAlater (Thermo Fischer Scientific, see Table 4) and kept at room temperature for 24 hours before stored at -80 °C until further processing. When adventitia and media were investigated separately, aortic tissue was transferred into an Eppendorf tube containing 1.0 ml Enzyme mix (see Table 4) and incubated at 37 °C for 20 min. Tissue was then transferred into a 5 cm^2 plate containing ice-cold Ringer solution. Using forceps, the

adventitia was separated from the media generally in one piece by pulling it off "like a sock". Media and adventitia were then placed into separate tubes containing RNAlater (Thermo Fischer Scientific, see Table 4).

Table 4. The list of chemicals and reagents

Name	Catalog No.	Manufacturer
Formafix 4 % gepuffert	F10010G	Grimm med. Logistik GmbH
RNAlater™-Solution	00990036	Thermo Fischer Scientific
Ethanol (70, 96 & 99 %)	79210-0006	Walter CMP
Xylol z. A.	326.2500	Th. Geyer GmbH & Co. KG
Hämatoxylin-Solution (Mayer)	1823101869	Medite GmbH
Eosin-Solution 0,2 %	11007528	Medite GmbH
Resorcin fuchsin-Solution nach Weigert 1%	362632	Waldeck GmbH & Co KG
Ferric-Hematoxylin A Weigert	15248	Waldeck GmbH & Co KG
Ferric-Hematoxylin B Weigert	13368	Waldeck GmbH & Co KG
Pikrinsäure-Solution 1,2 %	9C014641	AppliChem GmbH
Thiazinrot R	302526	Waldeck GmbH & Co KG
Isopropanol (70, 80, 85, 90, 96 & 100 %)	1136.5000	Th. Geyer GmbH & Co. KG
Tissue-Tek® Paraffinwachs TEK III	518881	Sakura Finetek Germany GmbH
Eukitt® Quick-hardening mounting medium	BCCB0745	Sigma-Aldrich Co. LLC.
Antigen Retrieval CITRA plus solution pH6	HK080-9K	BioGenex
Gibco 2-Mercaptoethanol	2216358	Thermo Fischer Scientific
Sodium chloride	S3014-1KG	Sigma-Aldrich Co. LLC.
Trizma® base	T1503-1KG	Sigma-Aldrich Co. LLC.
S1PR1 Rabbit-anti-human/mouse IgG 0,2 mg/ml	Sc-25489	Santa Cruz
CD31 rat-anti-mouse IgG 0,2mg/ml	DIA-310-M	Dianova
Isotype Control Rabbit IgG 5 mg/ml	GTX35035	GenTex
Isotype Control Rat IgG2a 1 mg/ml	MAB006	R&D
Fluoromount-G®	0100-01	Southern Biotech
Rabbit anti-rat IgG biotinylated	BA-4000	Vector Laboratories, Inc.
Antibody diluent	AL120R100	DCS
Antibody diluent	00-3218	Invitrogen
Dimethyl sulfoxide (DMSO) 500 ml	D4540	Sigma-Aldrich Co. LLC.

DAPI	6335.1	Carl Roth GmbH
H_2O_2 30%	437.1011	Th. Geyer GmbH & Co. KG
Donkey-Serum	S30	Merck Millipore
Rabbit-Serum	HK114-5K	BioGenex
Alexa Fluor® 594 Donkey-anti-Rabbit IgG	127803	Jackson ImmunoResearch
TBS (in 1L, pH 7.6)		
• Sodium chloride (8.8g) 150 mM	S3014-1KG	Sigma-Aldrich Co. LLC.
• Trizma base (6.1g) 50 mM	T1503-1KG	Sigma-Aldrich Co. LLC.
Enzyme mix		
Hank's balanced salt solution 500 ml	H6648	Sigma-Aldrich Co. LLC.
• Bovine Serum Albumin	A4378	Sigma-Aldrich Co. LLC.
• Soybean trypsin inhibitor 100 mg	LS003570	Worthington Biochemical Co.
• Elastase type III	E0127	Sigma-Aldrich Co. LLC.
• Collagenase 10 ku	LS005273	Worthington Biochemical Co.

2.2 Immunohistology

2.2.1 Paraffin embedding and cutting

Before embedding, the tissue was fixed and dehydrated following the procedures listed in Table 5. The infrarenal aorta was then cut transversely in the middle and both pieces were embedded with their cut side facing down next to each other with melted paraffin in metal cassettes (see Figure 6A). Following freezing at -20 °C, the solidified paraffin blocks were removed from cassettes and kept at -20 °C until further use.
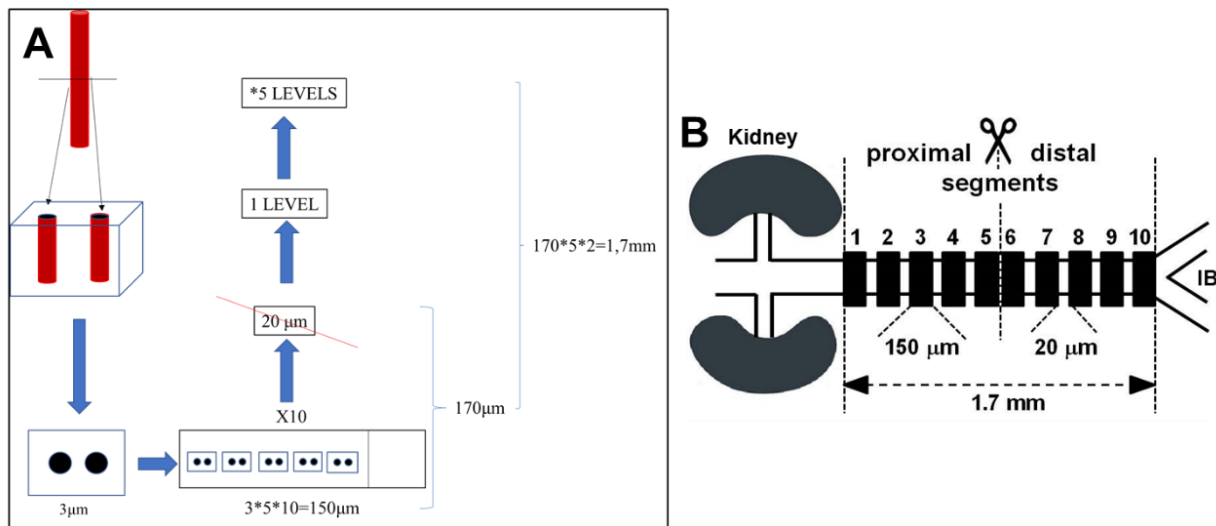
Figure 6. Illustration of paraffin embedding and cutting. Harvested vessels were cut in the middle and embedded with paraffin. 3 µm thick tissue sections were taken and 5 sections were put in one slide. After 10 slides (called one block level), 20 µm of tissue was discarded, followed by cutting another 10 slides **(A)**. In total 5 block levels or 10 aorta levels from proximal to distal in the order from 1 to 10 were generated for every vessel **(B)**. IB: iliac bifurcation.

Table 5. Procedure of tissue fixation and dehydration

Procedure	Time
4% Formalin	24 h
70% Isopropanol	20 min
70% Isopropanol	20 min
80% Isopropanol	20 min
85% Isopropanol	20 min
90% Isopropanol	20 min
90% Isopropanol	20 min
96% Isopropanol	20 min
96% Isopropanol	20 min
100% Isopropanol	20 min
100% Isopropanol	20 min
56 °C Paraffin	45 min

For staining, tissue sections (3 µm each) were cut from frozen blocks using a slide microtome (Leica Mikrosysteme Vertrieb GmbH): Five tissue sections were placed on a single microscope slide (Figure 6A). After cutting 50 sections yielding 10 slides, 20 µm

of tissue was discarded before collecting tissue sections again. Each of the 10 slides was called one block level including both proximal and distal parts of the same vessel. This way, 5 levels of blocks (with 10 slides each) also known as 10 levels of the whole vessel were generated for every infrarenal aorta (see Figure 6B).

2.2.2 Hematoxylin and eosin (H&E) staining

One slide for each block level including two aortic levels was stained with H&E. Slides were first deparaffinized in Xylene (Th. Geyer GmbH & Co. KG, see Table 4) three times for 5 min and then rehydrated first in 99% ethanol (Walter CMP, see Table 4) for 5 min twice, then one time in 96% ethanol for 5 min and finally one time with 70% ethanol for 5 min. The slides were rinsed quickly for several times in distilled water and incubated with hematoxylin (Medite GmbH, see Table 4) for 5 min. The slides were then washed with tap water for 10 min, rinsed with distilled water and incubated with 0.2% eosin (Medite GmbH, see Table 4) for 10 min. Excessive stain was removed by dipping slides first into 70% ethanol and then into 96% ethanol (Walter CMP, see Table 4). The slides were dehydrated by incubation in 99% ethanol (2 x 5 min) and cleared by incubations in xylene (3 x 5 min). Permanent mounting media (Sigma-Aldrich, see Table 4) was added to the tissue sections and a cover slip was carefully placed on top to avoid trapping air bubbles. The slides were then dried at room temperature overnight.

2.2.3 Elastic van Gieson (EvG) staining

Tissue slides were deparaffinized and rehydrated in ethanol as described in 2.2.2. Slides were then incubated with 1% Resorcin fuchsin (Waldeck GmbH & Co KG, see Table 4) for 25 min and excessive dye was washed away with tap water followed by

rinses with distilled water. Under the microscope (Karl Zeiss, see Table 7), tissue sections were differentiated by incubating with 70% ethanol until elastic fibers appeared dark purple. Differentiation was terminated by washing slides with water. The slides were then incubated with Weigert's Ferric-hematoxylin (Waldeck GmbH & Co KG, see Table 4) for 15 min, washed in tap water for 10 min and finally transferred into distilled water. Slides were then incubated with Thiazinrot R solution (Waldeck GmbH & Co KG, see Table 4) for 5 min followed by three dips each into distilled water, 70% ethanol and twice into 96% ethanol. Tissue sections were dehydrated in 99% ethanol for 2 x 5 min and cleared in xylene for 3 x 5 min. Permanent mounting media (Sigma-Aldrich, see Table 4) was added to the tissue sections and a cover slip was carefully placed on top to avoid trapping air bubbles. The slides were then dried at room temperature overnight.

2.2.4 Immunofluorescent staining for S1PR1

Tissue slides were deparaffinized and rehydrated in ethanol as described in 2.2.2. Slides were then incubated with Antigen Retrieval CITRA plus solution (pH 6, BioGenex, see Table 4) in a 95 °C water bath for 40 min before cooling down to room temperature while remaining in the antigen retrieval solution. Then the slides were washed in TBS (see Table 4) for 3 x 5 min. A grease pencil was used to encircle embedded tissues. Slides were then blocked with 5% donkey-serum (diluted in antibody dilution buffer (DCS, see Table 4)) (Millipore, see Table 4) for 20 min at room temperature and gently drubbed to remove blocking serum. Of the five section per slide (see 2.2.1), one was incubated with antibody diluent (DCS, see Table 4) for negative control, one with rabbit IgG (dilution 1:1250, GenTex, see Table 4) as isotype control and the remaining three sections were incubated with S1PR1 rabbit-anti-human/mouse IgG (dilution 1:50, Santa

Cruz, see Table 4) at 4 °C for overnight. Next day, the slides were first washed in TBS (see Table 4) for 3 x 5 min to remove antibody and then incubated with Alexa Fluor 594 Donkey-anti-Rabbit IgG (dilution 1:200, Jackson ImmunoResearch, see Table 4) at room temperature for 45 min followed by 3 x 5 min washes in TBS (see Table 4). Nuclei were stained by incubating slides with DAPI (4',6-Diamidino-2-phenylindol) solution (see Table 4) for 1 min at room temperature followed by washing them in TBS (see Table 4) for 5 min. Finally, Fluoromount-G media (Southern Biotech, see Table 4) was added to the tissue sections and a cover slip was carefully placed on top to avoid trapping air bubbles. The slides were then dried at room temperature for 30 min and then stored at -20 °C for further immunofluorescence microscopy (for method, see 2.4.2). All antibodies used in this protocol were diluted in antibody diluent (DCS, see Table 4).

2.2.5 Immunofluorescent staining for CD31

Tissue slides were deparaffinized and rehydrated and treated with antigen-retrieval solution as described above for S1PR1 staining (see 2.2.4). The slides were then incubated with 3% H_2O_2 (30% H_2O_2 (Th. Geyer GmbH & Co. KG, see Table 4) diluted in TBS) for 15 min to inhibit endogenous peroxide and washed in TBS for 3 x 5 min. Before primary antibody incubation, slides were incubated with Avidin for 15 min, washed in TBS for 3 x 5 min followed by an incubation with Biotin for 15 min and finally 3 x 5 min washes with TBS (see Table 4). Slides were blocked by a 20 min incubation in rabbit serum (BioGenex, see Table 4) and then gently drubbed to remove blocking serum. Of the five sections, one was incubated with antibody diluent (DCS, see Table 4) for negative control, one with incubated with rat IgG2a (dilution 1:125, R&D, see Table

4) as isotype control and the remaining three sections were incubated with CD31 rat-anti-mouse IgG (dilution 1:50, Santa Cruz, see Table 4) at 4 °C overnight. Next day, antibody was removed by washing slides in TBS (see Table 4) for 3 x 5 min. Then slides were incubated with biotinylated rabbit anti-rat IgG (dilution 1:200, Vector Laboratories, Inc. see Table 4) for 45 min and washed in TBS (see Table 4) for 3 x 5 min. Afterwards, slides were first incubated with streptavidin-conjugated horse radish peroxidase (HRP) (dilution 1:100, PerkinElmer, Inc. see Table 6) for 30 min, washed in TBS (see Table 4) for 3 x 5 min, then incubated with fluorescein tyramide reagent (dilution 1:50, PerkinElmer, Inc. see Table 6) for 3 min and washed in TBS (see Table 4) for another 3 x 5 min. The nucleus was stained by incubating slides with DAPI (see Table 4) for 1 min at room temperature and washed in TBS (see Table 4) for 5 min. Finally, Fluoromount-G media (Southern Biotech, see Table 4) was added to the tissue sections and a cover slip was carefully placed on top to avoid trapping air bubbles. The slides were then dried at room temperature for 30 min and stored at -20 °C for further immunofluorescence microscopy (for method, see 2.4.2). Primary antibodies and streptavidin-conjugated HRP all were diluted in antibody diluent (DCS, see Table 4), the biotinylated rabbit anti-rat IgG was diluted in antibody diluent (Invitrogen, see Table 4) and the fluorescein tyramide reagent was diluted in the amplification diluent (PerkinElmer, Inc., see Table 6).

Table 6. The list of research kits

Name	Components	Manufacturer
RNase-Free DNase Set	RNase-free DNase I RDD Buffer RNase-free Water	Qiagen GmbH
RNeasy Fibrous Tissue Mini Kit (50)	RNeasy Mini Spin Columns Collection tubes (1,5 ml) Collection tubes (2 ml) RLT Puffer Proteinase K RW1 Buffer RPE Buffer RNase-free Water	Qiagen GmbH
Maxima First Strand cDNA Synthesis Kit for RT-qPCR	5X Reaction Mix (Reaction buffer, dNTPs, oligo (dT)18, randomized Hexamer-Primer) Maxima Enzyme Mix (Maxima Reverse Transcriptase, RiboLock RNase Inhibitor) RNase-free Water	Thermo Fischer Scientific
Rotor-Gene® SYBR® Green PCR Kit (400)	2x Rotor-Gene SYBR Green PCR Master Mix (HotStarTaq®Plus DNA Polymerase, Rotor-Gene SYBR Green PCR Buffer, dNTP mix (dATP, dCTP, dGTP, dTTP))	Qiagen GmbH
Avidin & Biotin kit	Avitin Biotin	Life Technologies
TSA Fluorescein System kit	1X Amplification Diluent (15 ml) Fluorescein Tyramide (dry, dissolve in 300 µL DMSO) Streptavidin-HRP (150 µL) Blocking Reagent (3 g)	PerkinElmer, Inc.

2.3 Measurements of gene expression by real time quantitative polymerase chain reaction (RT-qPCR)

2.3.1 Ribonucleic acid (RNA) extraction of aortic tissue

RNA extraction was carried out with RNeasy® Fibrous Tissue Mini Kit (Qiagen GmbH, see Table 6) according to the manufacturer's instructions. For each run, material from two animals was pooled. Aortic tissues (whole vessels or separate media and adventitia) were extracted with 300 µL Buffer RLT supplemented with 3 µL β-Mercaptoethanol (Thermo Fischer Scientific, see Table 4) with two stainless steel

beads per tube using TissueLyser® LT (500 Hz, 4 × 5 min) (Qiagen GmbH, see Table 7). 590 µL RNase-free water and 10 µL proteinase K were added to the lysate. The mixture was incubated at 55 °C for 30 min and then centrifuged at 10,000×g for 3 min. The supernatant was transferred into a new tube and mixed with 450 µL of 99% ethanol. 700 µL of the sample was then transferred to a RNeasy Mini column which was placed into a 2 ml collection tube. The column was centrifuged for 1 min at 10,000×g, and the run-through discarded. These steps were repeated with the remaining sample. 350 µL Buffer RW1 was added to the column and centrifuged as above. 10 µL DNase stock solution was mixed with 70 µL Buffer RDD, the mixture was applied to the column which was then left for 30 min at room temperature. Afterwards, 350 µL Buffer RW1 was added to the column and the column was centrifuged for 60 s at 10,000×g followed by two washings steps with 500 µL Buffer RPE each. To elute the RNA, 50 µL RNase-free water was added to the column and the column was placed into a new 1.5 ml tube. The tube was centrifuged for 1 min at 10,000×g. The eluted RNA was stored at -80 °C until further use.

Table 7. The list of research instruments

Name	Catalog No.	Manufacturer
Centrifyge 5810	5810YR914582	Eppendorf AG
Thermomixer comfort	5355ZJ047028	Eppendorf AG
Leica SM2010R slide microtome	00001430	Leica Mikrosysteme Vertrieb GmbH
Zeiss standard 25 microscope	G/017997	Karl Zeiss
Bio-Rad T100™ Thermal Cycler	1861096	Bio-Rad laboratories, Inc.,
Roter-Gene Q real-time PCR cycler	9001550	Qiagen GmbH
Fluorescence microscope BZ 8100E		Keyence Deutschland GmbH
TissueLyser LT	06949	Qiagen GmbH
Spektralphotometer		BioTek Instruments, Inc.

2.3.2 RNA concentration measurements

To determine the concentration as well as the purity of RNA, the absorbance of the eluate (2 µL) was measured at 260 nm and 280 nm using an Epoch™ *Spektralphotometer* (BioTek Instruments, Inc, see Table 7). Nuclease-free water was used as a blank.

The data analysis software provided by the manufacturer for the spectrophotometer (Gen5TM 2.0, BioTek®) was used to calculate the sample RNA concentration and purity. RNA concentrations were calculated using the absorbance at 260nm by the Lambert-Beer's law (Dörr 1986):

$$E_{260} = \varepsilon_{260} * c * d \quad \rightarrow \quad c = \frac{E_{260}}{\varepsilon_{260} * d}$$

with $E_{260,}$ absorbance at 260 nm,

$\varepsilon_{260,}$ extinction coefficient for RNA at 260 nm (0.025 $(mg/ml)^{-1}cm^{-1}$)

$c,$ RNA concentration (mg/ml)

$d,$ length of light pass (1 cm).

2.3.3 RNA purity assessment

The purity of RNA was determined using the extinction quotient 260 nm/280 nm which ranges between 1.9 to 2.0 for pure RNA solutions (Gallagher and Desjardins 2001). RNA solutions at concentration below 1 ng/µL or with a 260/280 extinction quotient ≤1.5 or ≥2.5 were discarded.

2.3.4 Complementary deoxyribonucleic acid (cDNA) synthesis

The Maxima First Strand cDNA Synthesis Kit for RT-qPCR (Thermo Fischer Scientific, see Table 6) was used for DNA synthesis and reactions were carried out using a Bio-Rad T100™ Thermal Cycler (Bio-Rad laboratories, Inc., see Table 7) following the manufacturer's protocol. The Reaction Mix, Enzyme Mix and nuclease-free water were added together with template RNA into a sterile, RNase-free tube on ice (see Table 8).

Table 8. The reaction components for cDNA synthesis

Reagent	Volume
5X Reaction Mix	4 µL
Maxima Enzyme Mix	2 µL
Template RNA	200 ng
Water, nuclease-free	to 20 µL
Total volume	20 µL

Per assay, a maximum of 200 ng of total RNA was used. As the sample volume was 14 µL, RNA solutions were adjusted to 14.3 µg/ml using RNase free water. RNA solutions below 14.3 µg/ml were used without adjustments. After mixing, the tubes were centrifuged to collect all liquid and incubated as indicated in Table 9. The samples were incubated at 25 °C for 10 min followed by an incubation at 50 °C for 15 min. The reaction was terminated by heating the assay at 85 °C for 5 min. cDNA solutions were then cooled down and kept at 4 °C until taken out of the thermal cycler. cDNA samples were finally stored at -20 °C.

Table 9. The incubation procedure of cDNA synthesis

Temperature	Time
25 °C	10 min
50 °C	30 min
85 °C	5 min
4 °C	∞

2.3.5 Real time quantitative polymerase chain reaction (RT-qPCR)

All RT-qPCR reactions were carried out using Rotor-Gene® SYBR® Green PCR Kit (Qiagen GmbH, see Table 6) and a Roter-Gene Q real-time PCR cycler (Qiagen GmbH, see Table 7). SYBR Green I is an asymmetrical cyanine dye that preferentially binds to double-stranded DNA (dsDNA) and then emits 520 nm green light when absorbing 497 nm blue light. During the process of amplification, the fluorescence intensity of each cycle was measured and recorded by the cycler. The results were displayed in a fluorescence-cycle threshold (ct)-diagram. The ct value was determined by the cycle number corresponding to a preset fluorescence threshold and used to calculate the relative expression level of sample templates (for method see 2.3.6).

All primers (Sigma-Aldrich/Merck KGaA (Germany); desalted) including the housekeeping gene glyceraldehyde-3-phosphate dehydrogenase (GAPDH) used as reference gene are listed in Table 10. Primers (forward and reverse) were dissolved in nuclease-free water and adjusted to the concentration of 100 µM for storage. Stock solutions were diluted to 10 µM with nuclease-free water before use.

In each RT-qPCR run, 4 genes (3 genes of interest and the reference gene GAPDH) from 5 samples were measured in triplicates (60 reactions). In addition, for each gene, a negative control (water) was included (in duplicate, 8 reactions) and a positive control (5 pg/ml DNA fragments, 4 samples). The positive control are previously prepared

amplicons of the target genes using the same primers. Amplicons were then purified from agarose gels and their sequence was performed before use.

Table 10. The list of primers used for RT-qPCR

Gene	Forward Primer	Reverse Primer
S1PR1	5'-ATCATGGGCTGGAACTGCATCA-3'	5'-CGAGTCCTGACCAAGGAGTAGAT-3'
S1PR2	5'-CAGACGCTAGCCCTGCTCAAGA-3'	5'-TAGTGGGCTTTGTAGAGGA-3'
S1PR3	5'-ACAACCGCATGTACTTTTTCAT-3'	5'-TACTGCCCTCCCTGAGGAACCA-3'
Myh11	5'-ATGAGGTGGTCGTGGAGTTG-3'	5'-GCCTGAGAAGTATCGCTCCC-3'
Mouse CD68	5'-ACTTCGGGCCATGTTTCTCT-3'	5'-GGCTGGTAGGTTGATTGTCGT-3'
Mouse CD31	5'-TGCAGGCATCGGCAAAG-3'	5'-GCATTTCGCACACCTGGAT-3'
Mouse CD45	5'-GTTTTCGCTACATGACTGCACA-3'	5'-AGGTTGTCCAACTGACATCTTTC-3'
GAPDH	5'-TCCTGCACCACCAACTGCTT-3'	5'-AGGGGCCATCCACAGTCTTC-3'

A total of 72 reactions were loaded and analyzed in one run. Each reaction system contained the mixture of 1 µL of sample cDNA, 5 µL of SYBR green, 1 µL of diluted primer for the target gene and 3 µL of RNase-free water (Qiagen GmbH, see Table 11).

Table 11. The components of each RT-qPCR reaction

Reagent	Volume
RNase-free water	3 µL
Primers (Forward + Reverse; Concentration: 0,5 µM each)	1 µL
Rotor-Gene SYBR Green PCR Mastermix	5 µL
Sample	1 µL
Total volume	10 µL

The RT-qPCR reaction was carried out as shown in Table 12. Briefly, double stranded DNA was denatured at 95 °C before the temperature was decreased to 60 °C to allow annealing of primers. Elongation was then carried out at 72 °C. At the end of every run, a melting curve was recorded to identify reactions yielding multiple peaks which

indicates non-specific amplifications. Such reactions were discarded and measurements repeated with new solutions. In this situation, a new portion of the same cDNA sample and new reaction solutions along with primers were used to repeat another RT-qPCR procedure (see 2.3.5).

Table 12. The RT-qPCR reaction protocol

Step	Temperature	Time	Cycle
1. Initial Denaturation	95 °C	100 s	1 Repetition
2. Denaturation	95 °C	10 s	40 Repetition step 2 - 5
3. Annealing	60 °C	15 s	
4. Elongation	72 °C	20 s	
5. Melting curve	72 °C – 95 °C	5 s	

2.3.6 RT-qPCR data analysis

Data analysis of RT-qPCR measurements was carried out using the software Rotor-Gene, version 2.1.0.9 (Qiagen) and the calculation of gene expression (% GAPDH) using Microsoft Excel 2016 (see below).

Gene expression was given in percent GAPDH expression and calculated from the average ct values for each triplicate by the following formula (Livak and Schmittgen 2001):

$$\text{Target gene expression (\% GAPDH)} = 2^{-ct\,(\text{Target gene})-ct\,(\text{GAPDH})} * 100$$

For each calculation, the mean of all three individual ct-values was used. If the deviation between three individual ct-values of a triplicate was more than 0.5, measurements were repeated. If none of three measurements met this requirement, the mean of all nine individual ct-values was used. If any negative control yielded an

amplicon, or a positive control failed to be amplified, RT-qPCR measurements were repeated.

2.4 Histological analyses

2.4.1. Morphometric measurements

For morphometric analyses, one EvG-stained slide (for method see 2.2.3) from each block level was randomly chosen. As outlined in 2.2.1, every aorta was divided into 5 block levels, whereby one block level contained 2 aorta levels (one proximal and one distal) spanning the entire 10 aorta levels. This way, 10 measurements were taken for every aorta, spanning the entire length of the excised vessel. Slides were analyzed with a fluorescence microscope BZ 8100E (Keyence Deutschland GmbH, see Table 7) using the normal microscope mode. Tissue sections were photographed at a 100x magnification and analyzed using ImageJ software (NIH, USA).

Before measurement, the scale of the picture and parameters for the scale bar were entered. Four measurements were always taken, the length of and the area under the EEL and the IEL. If a neointima was visible, the length of lumen border and the lumen area were also determined. For measurements, the polygon selection-tool was used to manually draw along the selected lines. Once a circle was completed, both circumference and area were calculated and displayed by the computer (see Figure 7). When calculating morphometric parameters, one picture from each aortic level was processed individually and the mean value of all 10 aorta levels was finally presented in the form of mean ± standard deviation. Parameters including area of the media and intima/media ratio (I/M-ratio) were used in this study and the mathematical formulas are explained as follows:

The area of the media (A_{media}, μm^2) was then calculated by subtracting the area under the IEL from the the area under the EEL ($A_{media} = A_{EEL} - A_{IEL}$).

The area of the neointima (A_{lesion}, μm^2) was calculated by subtracting the lumen area from the area under the IEL ($A_{lesion} = A_{IEL} - A_{lumen}$).

The I/M-ratio is a parameter to evaluate the size of lesions. It is the quotient of intimal area (A_{lesion}, μm^2) and medial area (A_{media}, μm^2).

To calculate morphometric parameters, one picture from each aorta level was analyzed and the mean value of all 10 levels was then presented as mean ± standard deviation.

To investigate the distribution of a lesion, one section of each aorta level from mice at 28 days after surgery was used. In total, 120 sections from 12 mice were analyzed. A "1" was scored for every aorta level with a visible neointima.
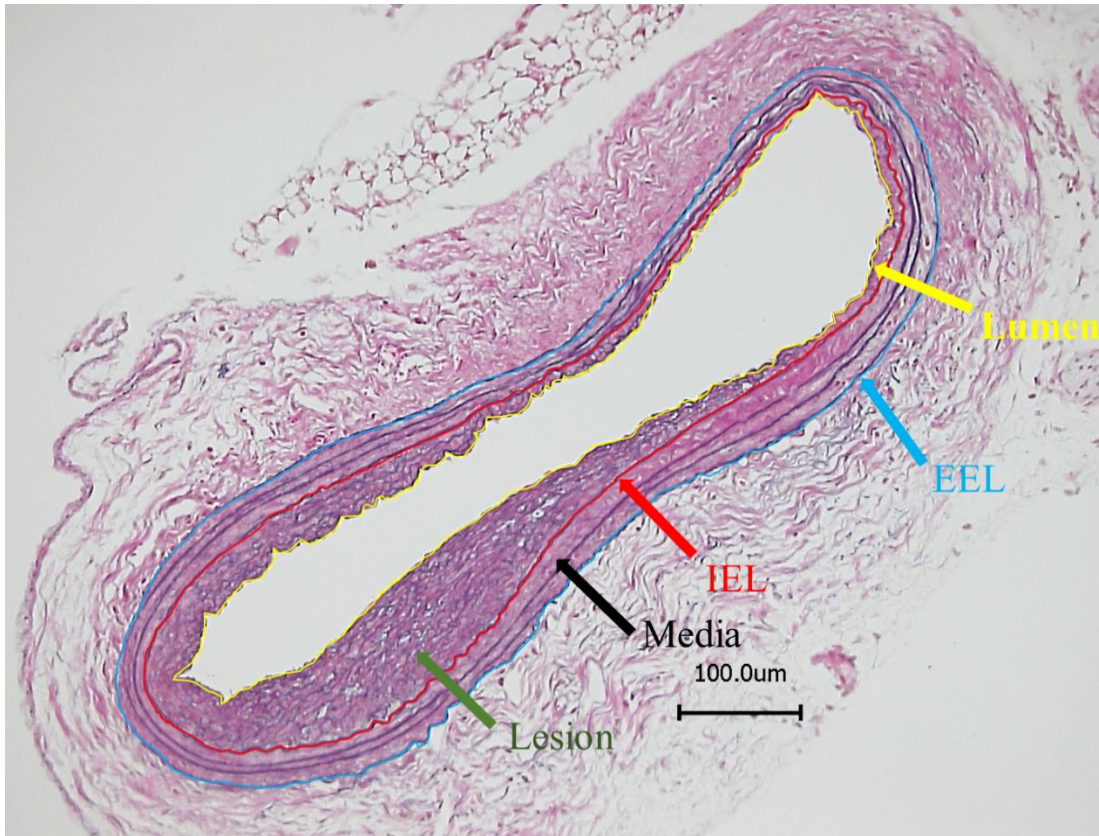
Figure 7. Illustration of morphological measurement. The infrarenal abdominal aorta segments were harvested from mice on day 28 after surgery and underwent EvG staining. Lesion formed between lumen and internal elastic lamina. IEL: internal elastic lamina; EEL: external elastic lamina; yellow line and arrow: outline of internal lumen; red line and arrow: outline of internal elastic lamina; bule line and arrow: outline of external elastic lamina; green arrow: representative lesion; black arrow: aortic media. Scale bar=100 μm.

2.4.2. Immunofluorescent microspcopy

For analysis of fluorescent dyes, the fluorescence microscope BZ 8100E (Keyence Deutschland GmbH, see Table 7) was used. For detection of CD31 (see 2.2.5), fluorescein tyramide was used (see Table 6, excitation at 492 nm, emission at 520 nm). For detection of S1PR1 (see 2.2.4), Alexa Fluor 594 was used (see Table 4, excitation at 590 nm, emission at 617 nm). For measurement of 4',6-Diamidino-2-phenylindol (DAPI), the excitation was at 358 nm and the emission at 461 nm. All photos were taken with a magnification of 100x.

2.4.3. Medial cell counts

For medial cell counts, nuclei were stained with DAPI (for method, see 2.2.4 or 2.2.5) and photographs (100x) were taken (for method, see 2.4.2). Nuclei were then counted manually using ImageJ software (NIH, USA). In the software, the IEL and EEL were firstly recognized in the photograph and then fields inside IEL and outside EEL were removed remaining media field only. The nuclei stained with DAPI were shown in bright blue dots under the black background and they were counted manually as the number of medial cells. For each artery, the mean values for all tissue sections were used.

2.5 Statistical analysis

Statistical analyses were carried out with Graph Pad Prism 5.0 (GraphPad Software Inc., La Jolla, USA). The data are presented as mean ± standard deviation (SD). For the comparison of two groups, t-test (two-sided) was used. For comparison of more than two groups, one-way ANOVA was used. $P < 0.05$ was considered statistically significant. More details are given in the figure legends.

3. Results

The first objective of this study was to establish a new mouse model for IH using the infrarenal aorta which generates sufficient tissue to facilitate a separate investigation of the I-M layer and the adventitia. The second objective was to apply this model to study the injury-dependent expression of S1P receptors (S1PRs) to identify possible novel functions of S1P/S1PRs in the arterial injury response.

3.1 Clamping of the infrarenal aorta induces IH

Clamping of the abdominal aorta was performed as described above (see 2.1.2). In total, 96 mice underwent this surgery. Two mice died during the procedure. To evaluate the extent of intimal lesions generated by this surgery, 12 mice were operated, sacrificed after 28 days and their infrarenal aortae were examined histologically. Twelve sham-operated mice were included where the aorta was dissected, but not clamped. Following excision, the vessels were processed for histology as described under 2.2.1. Each vessel was divided into 10 levels spanning its entire length. One tissue section per level was then histologically examined. None of the sham-operated animals showed any sign of a neointimal lesion while 11 out of 12 mice undergoing aortic clamping responded with IH (see Figure 8). Further, in none of the vessels (sham-operated or clamped) a thrombus or a rupture of the EEL or IEL was detected.
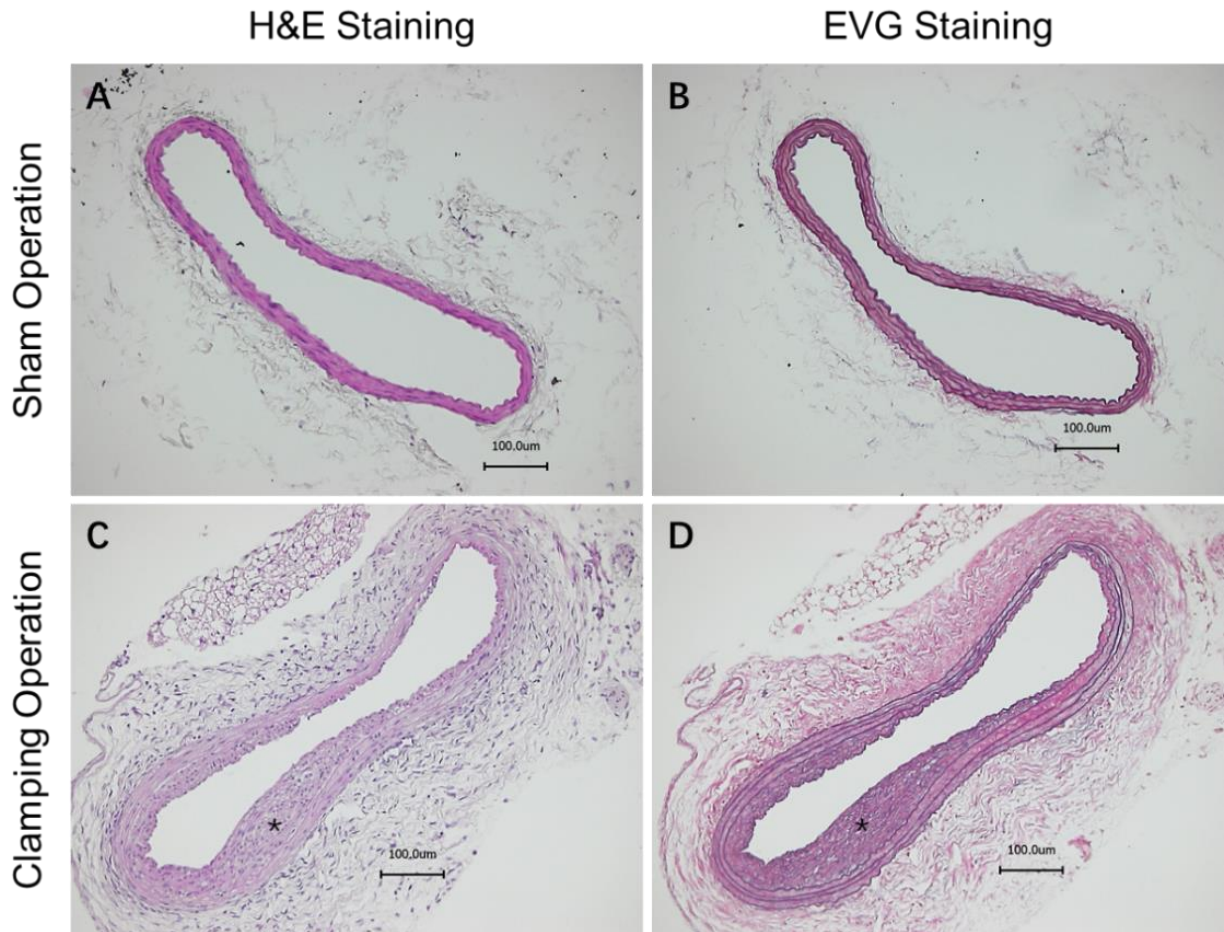
Figure 8. Histology of infrarenal abdominal aorta from both sham surgery and clamping surgery groups. Mice underwent sham operations (n=12) **(A, B)** or aortic clamping (n=12) **(C, D).** Vessels were harvested after 28 days and processed for histology, Sections were subjected to H&E staining **(A, C)** or EvG staining **(B, D)**. Representative tissue sections are shown. * Indicates presence of a neointimal lesion; Scale bars equal 100 µm.

3.2 Clamping causes endothelial denudation

To examine the effect of clamping on the integrity of the endothelial layer, infrarenal aortae were stained for CD31 before, immediately after and 4 days after clamping injury (for method see 2.2.5). Non-operated controls were included. Non-operated control vessels show a complete coverage with CD31-positive cells (Figure 9D). Immediately after clamping, an extensive loss of CD31 positive cells was observed (Figure 9E). After 4 days, the endothelial layer appeared almost completely restored (Figure 9H).
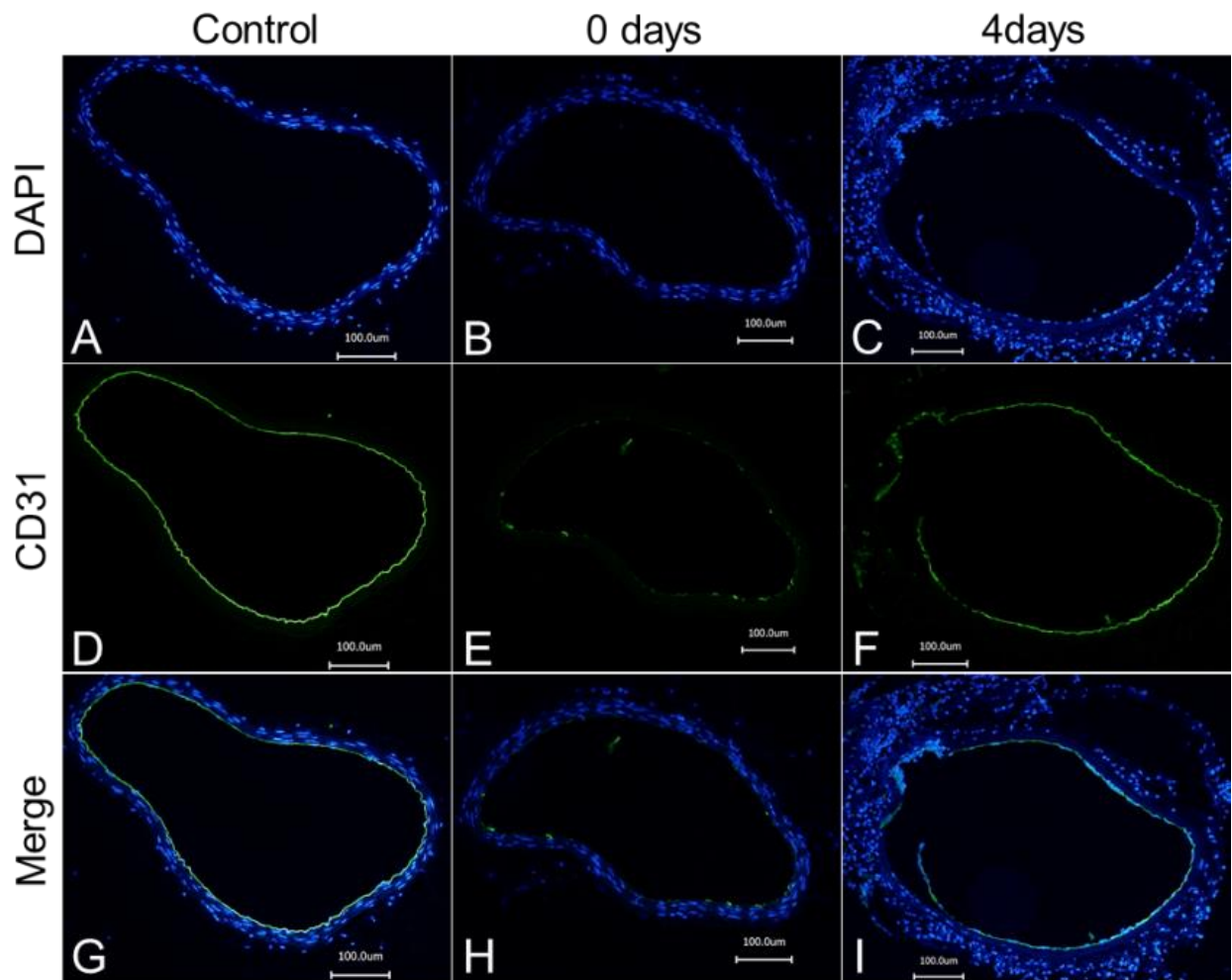
Figure 9. Time-dependent CD31 staining of IAA. Mice were subjected to aortic clamping. Vessels were excised immediately (0 days, n=4) **(B, E, H)** or at 4 days after clamping (n=4) **(C, F, I)**. Non-operated controls were included **(A, D, G)** Vessels were processed for histology and sections stained for CD31 **(D-I)** and DAPI **(A-C and G-I)**. Scale bars equal 100 μm.

3.3. Lesion distribution and morphometric analysis

To investigate whether lesions develop uniformly or at preferred sites, all sections (10 per vessel) of the vessels at 28 days after surgery (N=12) were first scored for the presence of a visible neointima (yes/no). The number of sections with a detectable lesion was then blotted against the position of the section (1=proximal end, 10=distal end, Figure 10A). This blot shows that most lesions form at the proximal part (Figure 10A). In a similar analysis, the I/M-ratio for every tissue segment was recorded (see 2.4.1) and the mean value of all sections per aorta level position was then blotted

against the position (Figure 10B). This analysis shows that in average, the largest lesion burden is also found at the proximal part of the aorta.

To investigate whether clamping injury causes changes in vessel circumference and media area, EVG stained slides from level 3 (for method see 2.2.1) where the largest lesion frequently formed were taken to measure the IEL and EEL circumferences. From these, medial areas were calculated (for methods see 2.4.1). Sham-operated animals (sh) were compared with clamped animals (cl). This analysis shows that both IEL and EEL circumferences and medial areas significantly increase after clamping (Figure 10C-E)
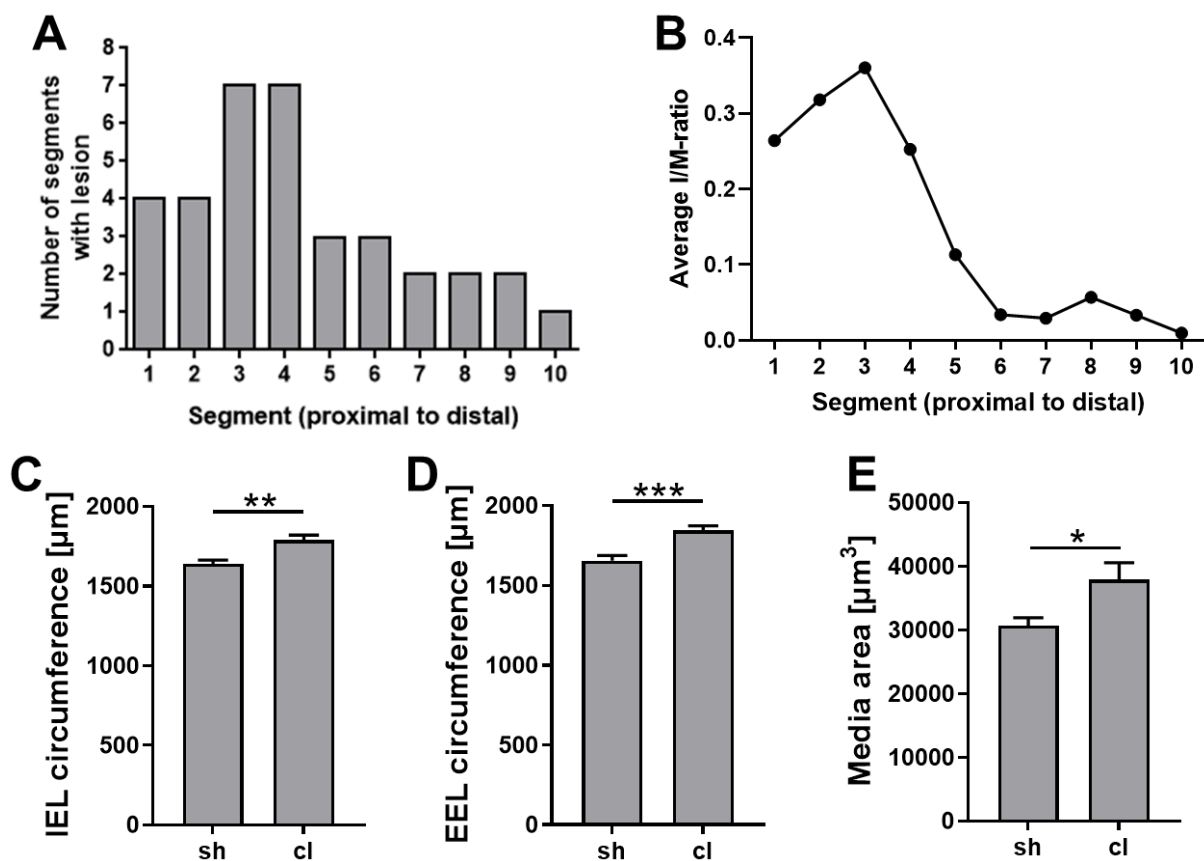

Figure 10. Lesion distribution and morphometric analyses. Mice underwent sham operations (n=12) or aortic clamping (n=12). Vessels were harvested after 28 days and processed for histology and sections were subjected to EvG staining. (**A**) For each aortic level (1-10), the number of segments with a neointima (0-12). (**B**) For each aortic level, the average I/M is shown. (**C**) The mean value of IEL circumference in segment 3 is presented (n=12). (**D**) The average EEL circumference in segment 3 is presented (n=12). (**E**) The mean value of media area in segment 3 is presented (n=12). sh: sham group; cl: clamping group; IEL: internal elastic laminar; EEL: external elastic laminar. *$p<0.05$, **$P<0.01$, ***$P<0.001$ (two-sided t-test).

3.4 Expression of cell markers

To investigate injury-dependent gene expression separately in the adventitia and the I-M, both layers were separated following a brief incubation of whole vessels in a protease mix (for method see 2.1.4). The expression of markers for VSMCs (MYH11), endothelial cells (CD31), macrophages (CD68) and leukocytes (CD45) were measured by RT-qPCR in the adventitia and I-M in non-operated controls, sham-operated or clamped infrarenal aortae at day 4 after surgery. For each measurement, two vessels were pooled (for method see 2.3.1). Expression data are given in percent expression of GAPDH, which was used as a reference gene. In non-operated controls, MYH11 and CD31 are found mainly expressed in the I-M (Figure 11A and 10B) whereas both CD68 and CD45 expression are almost completely restricted to the adventitia (Figure 11C and 10D). Sham operations cause MYH11 expression to decrease about 30% in the I-M and about 75% in the adventitia (Figure 11A). In contrast, CD31 expression in the I-M has a mild trend of decrease after sham surgeries, while in the adventitia, it increases two-fold (Figure 11B). Sham operations cause expression levels of CD68 (Figure 11C) as well as CD45 (Figure 11D) to greatly increase in the adventitia compared to non-operated control (co) and both markers are now detectable in the media as well. (Figure 11C and 11D). In the clamped aorta, changes already seen upon sham operations appear exacerbated (except for adventitial CD31 expression): in both arterial layers, MYH11 expression is further decreased (Figure 11A) and the expression of CD68 and CD45 is further increased (Figure 11C and 11D). Adventitial CD31 expression that increases upon sham operations appears unaltered in response to aortic clamping compared to non-operated controls (Figure 11B).
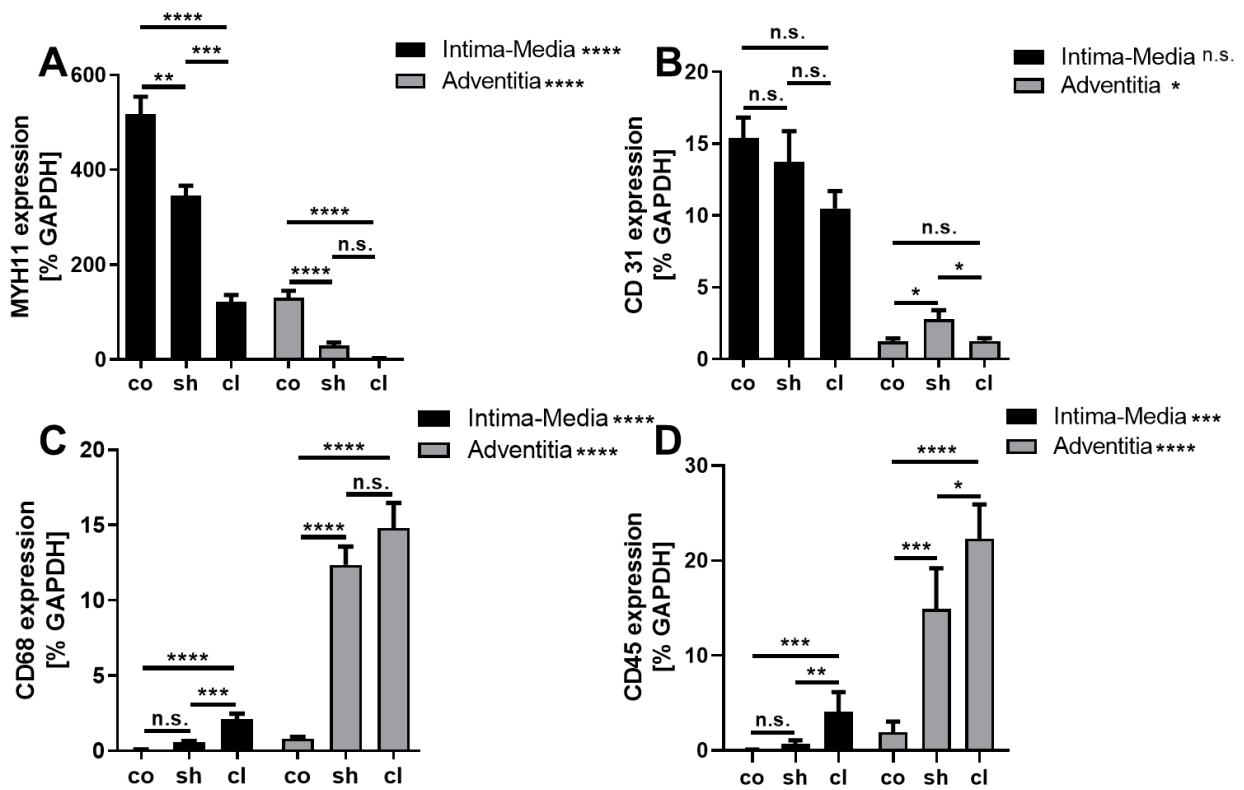
Figure 11. I-M and adventitial gene expression in infrarenal abdominal aortae. Mice were subjected to aortic clamping (cl, n=5 pools of 2 aortae each) or sham-operation (sh, n=5 pools of 2 aortae each). Non-operated mice were included as additional control (co, n=5 pools of 2 aortae each). At 4 days after injury, the infrarenal abdominal aortae were harvested and the adventitia separated from the I-M. Expression of MYH11 (A), CD31 (B), CD68 (C) and CD45 (D) was measured by RT-qPCR. Data (mean +/- SD) are shown for the I-M (black bars) and the adventitia (grey bars). *P<0.05, **P<0.01, ***P<0.001, ****P<0.0001 (one-way ANOVA test).

3.5 Surgery-dependent changes in medial cell numbers

To test the possibility that the loss of VSMCs contributes to the decreased MYH11 expression after surgery (see Figure 12A), cell counts were performed before and at 4 and 14 days after aortic clamping (for method see 2.4). The average cell number of all 10 levels to represent the entire abdominal aorta was assessed. This analysis shows that at 4 days after surgery, the number of medial cells decreased by more than 60% (Figure 12). At 14 days, cell numbers have increased to reach pre-surgical levels (Figure 12).
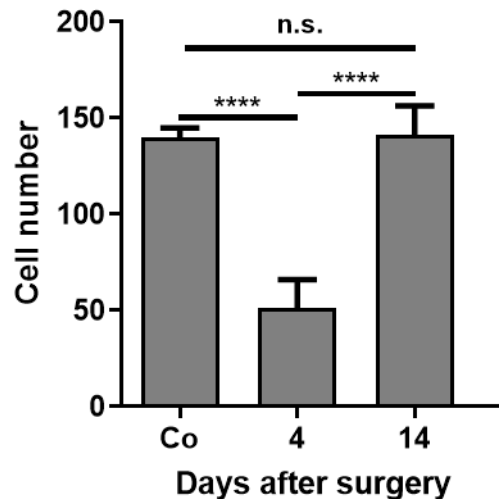
Figure 12. Surgery-dependent changes in medial cell numbers. Mice underwent aortic clamping and vessels were harvested at 4 (n=3) and 14 days (n=3). Non-operated controls (Co) were included (n=4). Vessels were processed for histology and tissue sections stained with DAPI. Sections of all 10 vessel levels were taken for cell number counting and the mean value of all 10 levels was presented for the result across the infrarenal abdominal aorta. The data of each group was compared respectively to other two group. ****P<0.0001 (one-way ANOVA test).

3.6 Injury-dependent expression changes of aortic S1P receptors.

To investigate the injury-dependent changes as well as the distribution of S1P receptor expressions in infrarenal aortae, mice underwent aortic clamping as described under 2.1.2. At 4 days after injury, vessels were harvested, I-M and adventitia were separated and both tissues were processed for RT-qPCR analysis. Non-operated controls were included. The expression levels of S1PR1, S1PR2 and S1PR3 were then measured by RT-qPCR. In non-operated controls, S1PR1 is higher expressed in the media when compared to the adventitia, S1PR2 is higher expressed in the adventitia and S1PR3 is equally expressed in both vessel layers (Figure 13). Upon injury, the expression of S1PR1 increases in both I-M and adventitia by nearly two-fold (Figure 13A) while the expression of S1PR2 in the I-M remains unchanged but decreases by 50% in the adventitia (Figure 13B). For S1PR3, expression changes for the I-M and the adventitia

are opposite in that it decreases by more than 50% in the IM and increases about 4-fold in the adventitia (Figure 13C).
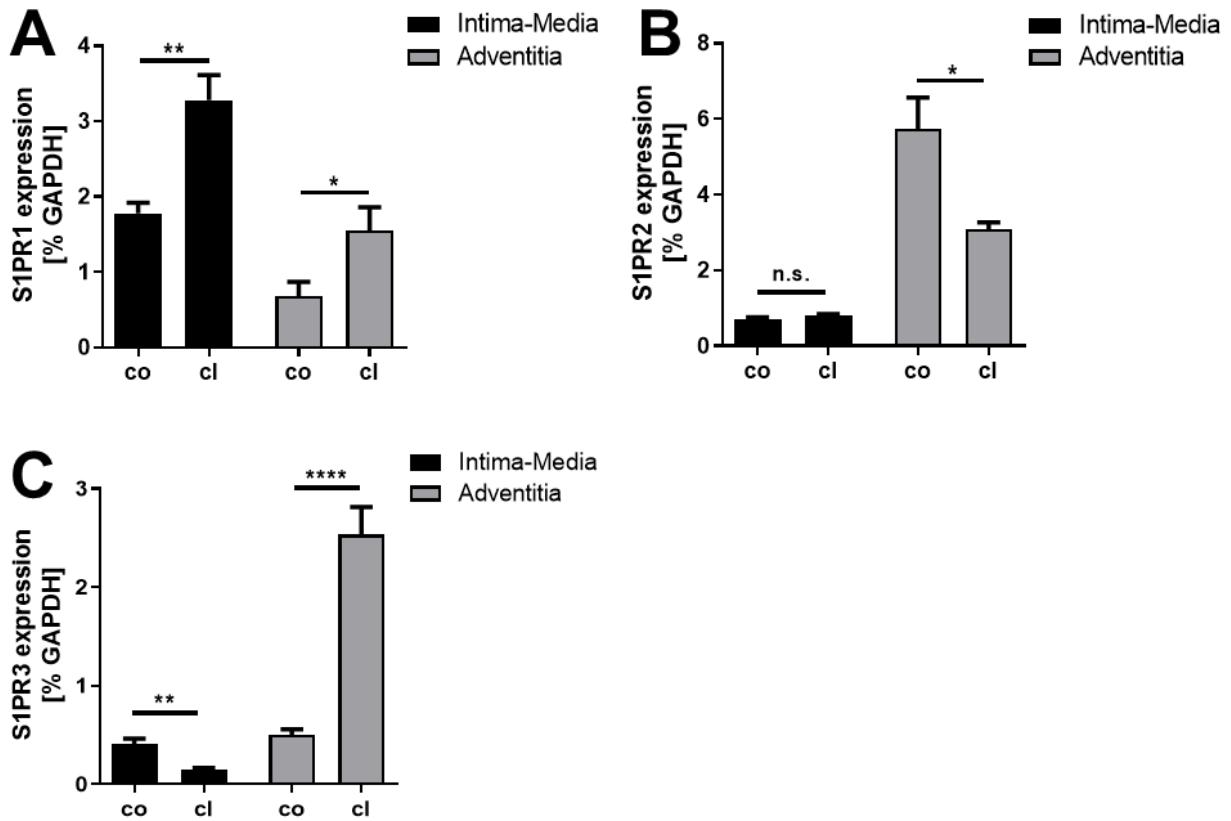

Figure 13. I-M and adventitial S1PRs expression in infrarenal abdominal aortae. Mice were subjected to aortic clamping (cl, n=5 pools of 2 aortae each). Non-operated mice were included as control (co, n=5 pools of 2 aortae each). At 4 days after injury, aortae were harvested and the adventitia separated from the I-M. Expression of S1PR1 **(A)**, S1PR2 **(B)** and S1PR3 **(C)** was measured by RT-qPCR. Data (mean +/- SD) are shown for the I-M **(black bars)** and the adventitia **(grey bars)**. *P<0.05, **P<0.01, ****P<0.0001 (two-sided t-test).

3.7 Immunohistological analysis of S1PR1 expression

To investigate injury-dependent changes in the distribution of S1PR1 positive cells, sections across the entire length of infrarenal aortae were stained with S1PR1 before, immediately after, and at 4 days, 14 days and 28 days after clamping (for method see 2.2.4). To analyze S1PR1 expression, slides from level 3 (for method see 2.2.1) were used. In non-operated controls, S1PR1-positive cells were found in all arterial layers

(Figure 14F and 14P). Immediately after clamping, S1PR1 positive cells are no longer detectable in the intima (Figure 14G and 14Q). At 4 days after injury, the intima, which at that time consists of mainly endothelial cells (see chapter 3.2 and Figure 9), stains positive for S1PR1 again. Generally, a loss of cells was observed in the media at 4 days after injury (see chapter 3.6, Figure 12) concomitant with an apparent decrease of S1PR1 staining (Figure 14H and 14R). In contrast, adventitial staining for S1PR1 is more intense at 4 days after clamping when compared to non-operated controls (Figure 14F and 14P vs. Figure 14H and 14R). Between 4 and 14 days after injury, the numbers of S1PR1 positive cells have increased in the media and adventitia (Figure 14H and 14R vs. Figure 14I and 14S). Moreover, the now expanded neointima mainly consists of S1PR1 positive cells (Figure 14I and 14S). At 28 days after injury, overall staining for S1PR1 in the media appears less intense, but is still strong in the neointima and the adventitia (Figure 14J and 14T).
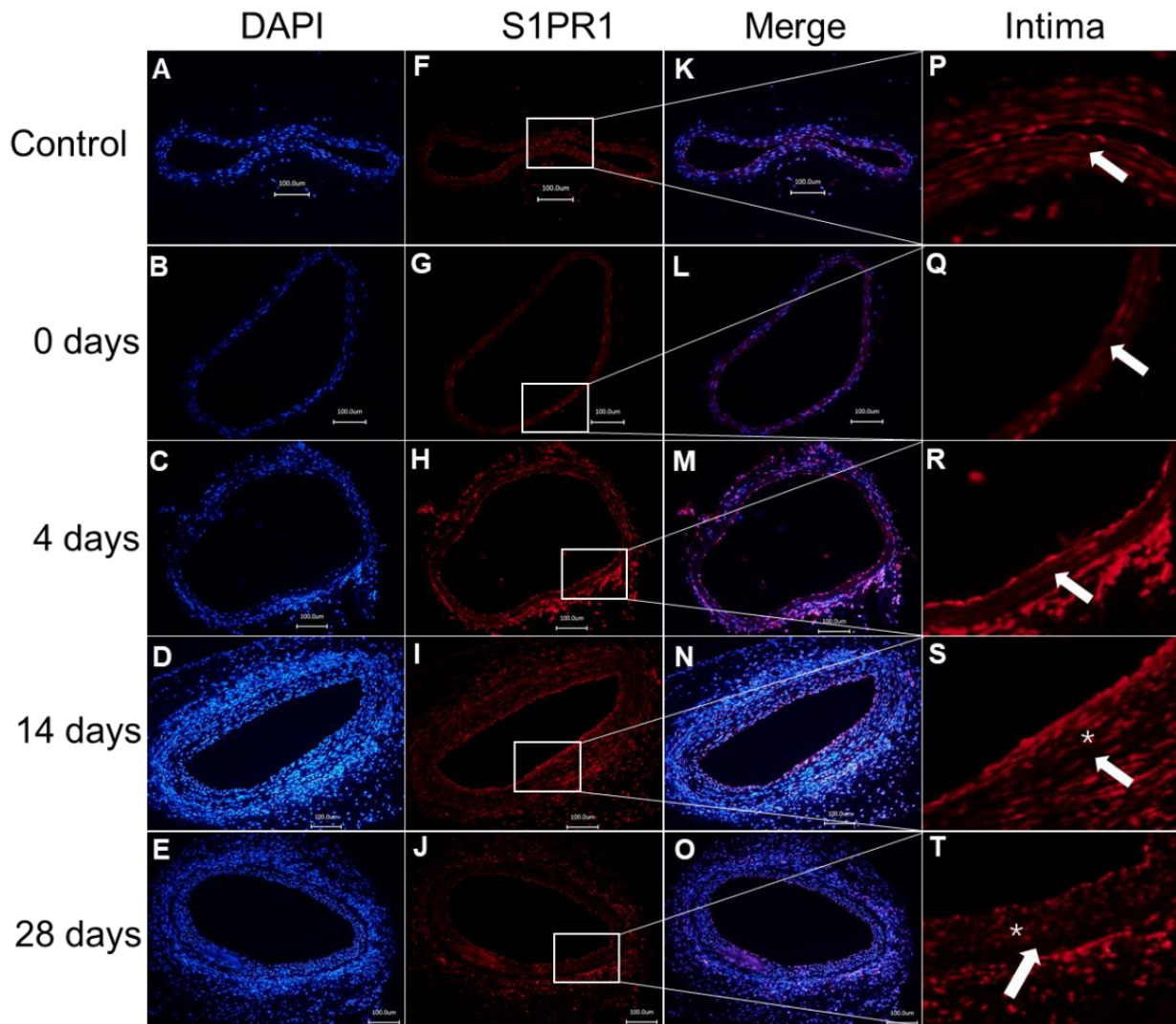
Figure 14. Time-dependent S1PR1 staining of IAA. Mice were subjected to aortic clamping (Each time point, n=3) or non-operated (Control, n=3). Immediately after injury (day 0) or at 4, 14 and 28 days after injury, infrarenal aortae were harvested, processed for histology and stained for S1PR1.and with DAPI as indicated. For this analysis, only slides from level 3 were used. For every time point, staining for DAPI (**A, B, C, D, E**), S1PR1 (**F, G, H, I, J**), and both (Merge) is shown. (**K, L, M, N, O**). In addition, a magnified section depicting S1PR1 staining in the intima is presented (**P, Q, R, S, T**). Arrows point onto the arterial media between internal and external elastic lamina; Stars point onto the neointima lesions. Scale bars equal 100 μm.

3.8 Clamping of infrarenal aorta affects the expression of MYH11 and CD68 in the proximal aorta.

Here, the possibility was tested that clamping of the infrarenal aorta affects the expression of MYH11 or CD68 in the proximal aorta. Therefore, following clamping of the infrarenal aorta, the aortic arch and the thoracic descending aorta were also

49

harvested and processed for RT-qPCR analysis. Upon injury, when MHY11 expression significantly decreases in the injured infrarenal aorta (see chapter 3.5, Figure 11A), it increases in the media of both the aortic arch and descending thoracic aorta (Figure 15A and 15C). Adventitial expression of CD68 significantly increases in the thoracic aorta when the infrarenal aorta was injured (Figure 15B). A trend in the same direction was observed for the aortic arch (Figure 15D). No changes were observed for adventitial MYH11 or medial CD68 (Figure 15).
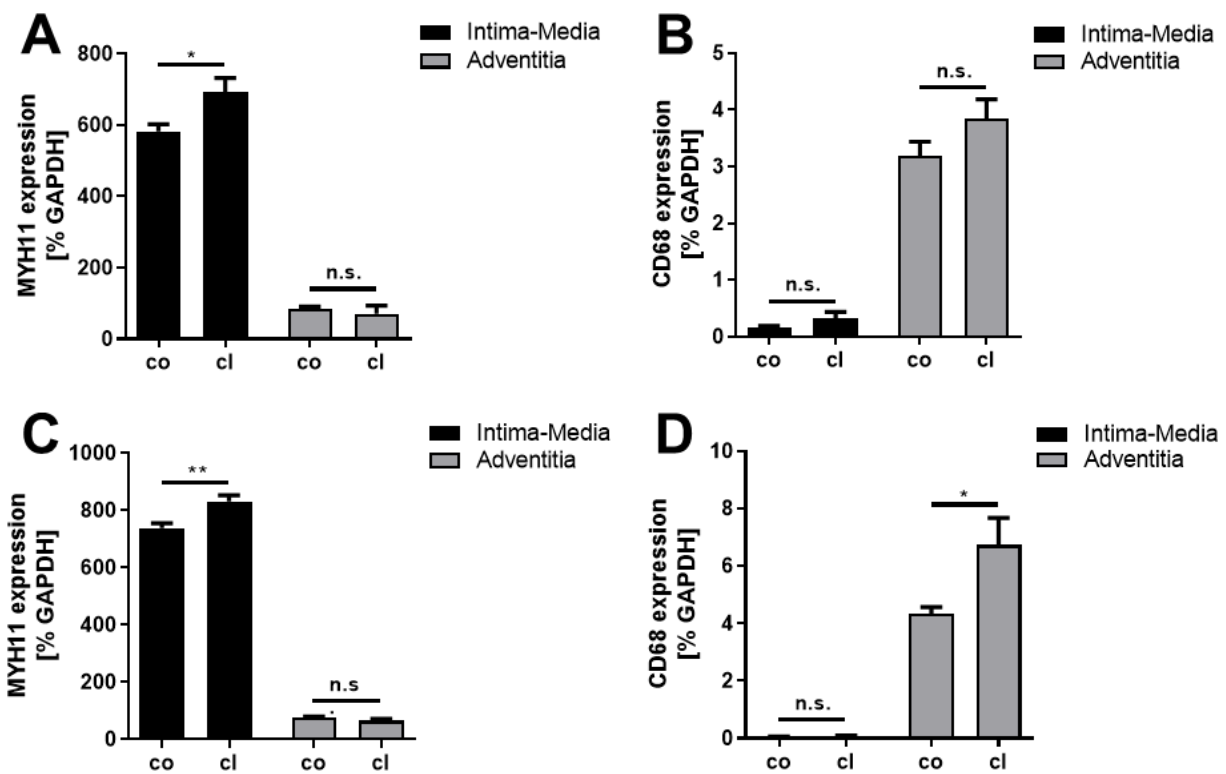

Figure 15. I-M and adventitial gene expression in the aortic arch and the thoracic aorta following clamping the abdominal aorta. Mice were subjected to aortic clamping (cl, n=5 pools of 2 aortae each). Non-operated mice were included as control (co, n=5 pools of 2 aortae each). At 4 days after injury, the aortic arch and thoracic aorta were harvested, the adventitia separated from the I-M and both tissues processed for RT-qPCR analysis. Expression of MYH11 **(A)** and CD68 **(B)** in the aortic arch and of MYH11 **(C)** and CD68 **(D)** in the thoracic aorta was measured by RT-qPCR. Data (mean +/- SD) are shown for the I-M **(black bars)** and the adventitia **(grey bars)**. *P<0.05, **P<0.01 (two-sided t-test).

4. Discussion

4.1 Restenosis

With the further development of surgical and interventional techniques, restenosis rates are decreasing but still remain a serious limitation for vascular procedures (Aoki and Tanabe 2021, Miura et al. 2021). Although intimal hyperplasia is one of the major causes for restenosis, underlying mechanisms are not fully understood yet. Here, we establish a mouse model for IH using the abdominal aorta which yields sufficient tissue to easily analyze the I-M and adventitia separately. Our analyses mainly focused on the distinct expression changes of S1P receptors in response to injury.

4.2 Aortic clamping is a suitable model to study IH

Existing mouse models for IH including carotid ligation and femoral denudation have various limitations. A major limitation of these models is the small size of murine carotid and femoral arteries as for gene expression experiments, especially when both adventitia and media are separately investigated, arteries have to be pooled and 10-15 animals sacrificed for a single data point.

Notably, the femoral denudation surgery requires advanced surgical skills and is quite challenging. Despite the comparably easy surgery of carotid ligation, thrombus formation has been frequently reported in response to this procedure which may confound results obtained (Abarbanell et al. 2010). We therefore sought to further explore a recently reported mouse model involving clamping of the abdominal aorta for its suitability of studying IH (Shirali et al. 2016). This model was shown to cause aortic denudation but long-term outcomes such as IH have not yet been investigated. To us,

this model offers several advantages. The major one is the relatively large size of the abdominal aorta that allows easy separation of the adventitia from the media on one hand, and on the other, sufficient material is obtained to save a large number of animals compared to the use of carotid or femoral arteries. In general, pooling two arteries was sufficient for one data point. Another advantage is the apparent rarity of severe thrombosis as we have never observed occluding thrombi at 28 days after surgery in any of the 12 mice investigated. Most importantly, we found that in 11 out of 12 mice that underwent aortic clamping a noticeable neointima had developed within 4 weeks after surgery (Figure 8).

During the surgery, clamping is performed uniformly across the entire infrarenal abdominal aorta as every segment of the aorta undergoes triple clamping (see 2.1.2). Nevertheless, lesions develop preferentially at the proximal end of the aorta (Figures 10A and 10B). One explanation for this observation may lie in locally disturbed flow conditions caused by arterial bifurcations in the proximal part of the infrarenal aorta including left and right spermatic arteries (Aslanidou et al. 2016). Generally, bifurcations generate disturbed flow and cause low shear stress which impairs endothelial cell (EC) functions such as nitric oxide (NO) generation and NO inhibits VSMC proliferation (Tseng et al. 1995). This change of shear stress has been shown to promote IH, e.g., in a graft transplantation model (Mattsson et al. 1997). In this study a polytetrafluoroethylene (PTFE) graft was transplanted between iliac and infrarenal aortas in baboons to create a low shear stress environment and the result showed larger lesion was formed in the graft.

At 28 days after injury, positive remodeling has been observed indicated by an increase of outer and inner arterial circumferences (Figures 10C and 10D). In addition, increased medial area was also found (Figure 10E) which may be due to migration and

proliferation of VSMCs (Newman et al. 2018). Production of a proteoglycan-rich matrix may also contribute, which further expands by binding water (Rensen et al. 2007).

4.3 Aortic clamping causes endothelial denudation, loss of medial VSMCs and adventitial inflammation

Possible triggers of neointimal hyperplasia in our clamping model includes endothelial denudation, medial cell loss by apoptosis and adventitial injury-induced inflammation. Endothelial cells keep VSMCs in a quiescent state by producing growth inhibitors such as NO and prostacyclin. (Patel et al. 2010, Bath et al. 1991). Injury-mediated loss or damage of the endothelial layer results in the infiltration of the wall by leukocytes and macrophages that produce cytokines stimulating VSMC proliferation and migration (Welt and Rogers 2002, Nomoto et al. 1988). The observation that delayed re-endothelialization is associated with larger neointimal hyperplasia is consistent with an inhibitory role for ECs in SMC proliferation and migration (Zhang et al. 2013).

Cell counting showed that the clamping injury causes a significant loss of medial cells at 4 days. Although we have not investigated the underlying processes, we assume that apoptosis plays a role as has been previously shown in other models of arterial injury (Bennett 1999). Injury induced arterial VSMC apoptosis is an early event after injury (Walsh et al. 2000). For example, after denudation of the mouse femoral artery, apoptotic cells have been detected in the media as early as at 2 hours after injury followed by a measurable decrease of medial cell numbers at 17 hours (Sata et al. 2000). It is assumed that during this early wave of apoptosis, dying cells release cytokines such as Interleukin 1 (IL-1) which promote VSMC proliferation (Miwa et al. 1998). In the present study, loss of medial cells was observed at 4 days after injury,

whereby at 14 days, the media appeared completely repopulated (Figure 12). Interesting questions remain to which extent VSMCs die by apoptosis in this model and also whether adventitial cells play a role in repopulating the media.

The increased expression of cell markers for macrophages (CD68) and leukocytes (CD45) in the adventitia indicates an injury-induced adventitial inflammation response which we assume to contribute to IH. A role for the adventitia in neointima formation has been previously reported in several animal models including porcine and rabbit arteries where removal or damage of adventitial tissue resulted in VSMC proliferation and migration (Wilcox and Scott 1996). Interestingly, when porcine coronary arteries are wrapped with a cotton mesh containing IL1β, the vessels respond with neointimal growth (Shimokawa et al. 1996). In a sheep dialysis access failure model, when the graft connecting the left common carotid artery and right external jugular vein was covered with anti-inflammation paclitaxel-eluting mesh neointimal lesion formation was decreased (Kohler et al. 2007). Together, these studies indicate that adventitial inflammation is a major contributor to VSMC activation and intimal growth.

4.4 Sham-operated animals do not generate neointimal lesions

Unlike in mouse models involving carotid or femoral arteries, in the aortic clamping model, there is no contralateral vessel that could be used as an internal control. We have therefore considered three experimental groups involving non-operated controls, sham-operated (vessel preparation only) and clamped. The purpose of the sham-operated group was to investigate effects of the preparative procedures and compare those to the clamping injury. Morphometric analyses show that sham-operated animals do not generate lesions at 28 days (Figure 8A and 8B).

4.5 Injury-induced changes of cell marker expression in adventitial and I-M layers

To monitor alterations of cell marker expression in the adventitia and I-M induced by injury, the two layers were separated immediately after excision of the aorta (see 2.1.4). By RT-qPCR (see 2.3), we then measured the expression of the VSMC marker Myh11, the endothelial cell marker CD31, the monocyte/macrophage marker CD68 and the leukocyte marker CD45. As expected, in non-operated controls, Myh11 and CD31 are expressed much higher in the I-M than in the adventitia which also confirms the successful separation of the two vessel layers (Figure 11A and 11B). Adventitial expression of Myh11 and CD31 may stem from the vasa vasorum, but adventitial VSMCs, lymphatic ECs and endothelial progenitor cells may also contribute to adventitial expression of these genes. The source of adventitial expression of CD68 and CD45 are likely resident macrophages and leukocytes (Stenmark et al. 2013), Notably, expression levels of CD68 and CD45 were almost undetectable in the I-M confirming the absence of inflammatory cells in this aortic layer without injury.

At 4 days after clamping injury Myh11 expression decreases in both layers when compared to non-operated controls. In the I-M layer, this may be a consequence of decreased cell numbers which we observed in cell counts (Figure 12). As discussed above (see 4.3), this may be due to injury-induced apoptosis. Another interpretation for the decreased expression of Myh11 in injured aortae is the de-differentiation of VSMCs. Generally, arterial injury causes VSMCs to change from a contractile to a synthetic phenotype and this process is characterized by decreased expression of VSMC-specific genes (Rensen et al. 2007). This phenotypical transition resulting in increased cell proliferation and matrix production is possibly a major cause for the observed increase in medial size (Figure 10E). Unexpectedly at first, given that clamping removes the endothelium (see Figure 9), CD31 expression at 4 days after injury was

not significantly lower when compared to non-operated controls (Figure 11B). The possibility that by then, the endothelial layer had regrown was confirmed by CD31 staining showing an approximate 90% endothelial coverage at 4 days after injury (Figure 9). Aortic clamping induces a strong increase of adventitial expression of CD68 and CD45 indicating an inflammatory response (Figure 11C and 11D). Macrophages and leukocytes are apparently quickly recruited upon injury. At 4 days after injury, the inflammatory cell markers CD68 and CD45 are also detectable in the I-M of the injured aorta and we consider it likely that invading cells not only stem from the circulation but also from the adventitia (Figure 11C and 11D).

In the sham-operated group, we have also observed injury-induced expression changes of cell markers. The Myh11 expression in both layers decreases compared to non-operated controls but is still higher than in injured vessels (Figure 11A). Obviously, preparing of the aorta which involves cutting and tearing apart connective tissue may cause adventitial VSMC death or trigger de-differentiation similar to clamping injury, but to a lesser extent. Adventitial CD31 expression in the sham-operated group was found to increase, which was an unexpected observation. The reason herefore is unclear but one interpretation could be that adventitial endothelial progenitor cells (EPCs) expand in response to the dissection injury. EPCs can differentiate into endothelial cells in response to VEGF in vitro (Xu 2005). In a mouse vein graft transplantation model, a wild-type vein graft was transplanted into the carotid artery of a TIE2-LacZ mouse and it was shown that the endothelium of the vein graft was regenerated by recipient bone marrow EPCs (Xu et al. 2003). Such increase of EPCs may not be detectable in clamping as adventitial injury here is much stronger compared to sham operations and cells may be physically damaged or killed. Like clamping, also sham-operations alone cause a strong increase in the expression of adventitial CD68 and CD45, but with

expression levels still below those seen in clamped vessels (Compare Figure10C and 10D). Nevertheless, adventitial injury inflicted by dissecting the aorta is sufficient to induce an obviously robust inflammatory response. Importantly, we have never observed neointimal growth in sham-operated animals at 28 days after surgery (Figure 8A and 8B). In summary, except for CD31, sham operations cause similar though less pronounced changes of cell marker expression compared to aortic clamping.

4.6 Injury-induced changes of S1P receptor expression in I-M and adventitial layers

Although a role for S1P/S1PRs in the arterial injury response has been suggested by many studies (see 1.5.3), at present, no information is available regarding any S1P/S1PR signaling domain in the adventitia that may regulate injury-induced IH. To start addressing this point, we measured S1P receptor expression in both, the adventitial as well as the I-M layer in our aortic clamping model. Regarding the I-M layer, it is generally assumed that S1PR1 is highly expressed by ECs, while S1PR2 and S1PR3 are mainly expressed by VSMCs and fibroblasts (Ouyang et al. 2020). In healthy mouse aortae, S1PR1 shows a nearly two-fold higher expression in the I-M than in the adventitia (Figure 13A). Staining aortic tissue sections for S1PR1 confirms its expression by ECs, medial VSMCs and also adventitial cells, probably resident leukocytes as well as fibroblasts (Figure 14P) (Liu et al. 2000, Galvani et al. 2015). After clamping injury, both I-M and adventitial S1PR1 expression increases (Figure 12). Notably, S1PR1 staining indicates that the vast majority of neointimal cells express S1PR1 at 14 days (Figure 14). Possibly, S1PR1 is expressed by activated VSMCs to promote migration and proliferation. Similar observations were made in a humanized IH

model, where a denuded human IMA was transplanted into immuno-deficient rats in the position of the abdominal aorta (Braetz et al. 2018). In this model, denudation of the transplanted IMA triggered medial as well as intimal proliferation accompanied by the appearance of S1PR1-positive cells. Another study showed that treatment with the S1PR1 antagonist VPC44116 in a mouse carotid balloon injury model attenuates lesion formation (Wamhoff et al. 2008). Taken together, these observations suggest that S1PR1 signaling promotes neointimal hyperplasia by activating VSMC proliferation and migration.

Clamping injury also increases adventitial S1PR1 expression which may point to an activation of adventitial cells (Figure 13A). Possible S1PR1-positive cells include inflammatory cells (monocytes, macrophages), fibroblasts or myofibroblasts. Double staining experiments should be performed in the future to identify S1PR1-positive adventitial cells types. Notably, adventitial fibroblasts have been shown to differentiate into myofibroblast in response to injury (Havelka and Kibbe 2011). Part of this process may be S1PR1 expression that enables myofibroblasts to migrate towards the I-M. Injury-induced migration of adventitial cells has previously been described, e.g., in rat carotids following balloon injury (Siow et al. 2003).

In the uninjured abdominal aorta, adventitial S1PR2 expression is much higher than expression in the I-M (Figure 13B). After injury, a decrease of S1PR2 expression was observed in the adventitia. S1PR2 couples to $G_{\alpha 12/13}$ and activates Rho which inhibits cell migration (Ridley 2015). In the mouse carotid ligation model, S1PR2 knock-out mice generate much larger lesions than wild-type animals. Cell culture experiments showed that S1PR2 knock-out VSMCs show increased migration in the presence of S1P when compared to wild-type cells (Shimizu et al. 2007). Similar observations were made in fibroblasts where deletion of S1PR2 promotes migration and proliferation via

activation of Rac and SphK1 (Goparaju et al. 2005). Together, these findings support the conclusion that decreased adventitial S1PR2 expression promotes adventitial cell migration and proliferation following arterial injury. Besides inhibiting VSMC migration, S1PR2 has also been shown to promote the expression of SMC genes including smooth muscle alpha-actin (SMA) in a Rho-dependent manner (Grabski et al. 2009). As over-expression of SMA inhibits VSMC proliferation and migration (Chen et al. 2016), we conclude that S1PR2 is keeping adventitial fibroblast or myofibroblasts in a quiescent state and that injury-induced suppression of S1PR2 then enables these cells to expand and to migrate towards the forming neointima. As S1PR2 also plays a negative role in macrophage migration (Michaud et al. 2010), loss of S1PR2 expression upon injury may promote the ability of adventitial macrophages to invade the media.

In non-operated controls, S1PR3 appears to be equally strong expressed in both aortic layers (Figure 13C). Interestingly, clamping injury has opposing effects on S1PR3 expression in the two layers, it decreases in the I-M and increases in the adventitia (Figure 13C). Similar to the interpretation of the changes of Myh11 expression (see above), the injury-induced decrease of S1PR3 expression in the I-M may also be due to the loss of cells or due to VSMC de-differentiation (Figure 12). Notably, a significant increase of adventitial S1PR3 expression was found after injury possibly indicating an important role for this receptor in adventitial cell regulation (Figure 13C). Previous experiments with VSMCs over-expressing S1PR3 showed that S1PR3 expression is associated with increased migration and proliferation (Shimizu et al. 2012). In addition, S1PR3 is also involved in regulating cell differentiation. In tissues culture experiments, activation of S1PR3 and Smad3 signaling has been shown to promote the transdifferentiation of fibroblast into myofibroblast (Keller et al. 2007). Moreover, S1PR3 can also induce mesenchymal stem cells to differentiate into VSMC-like cells (Nincheri

et al. 2009). The role of S1PR3 in IH was previously investigated in two different mouse models with opposite results. Compared to wild-type animals, S1PR3 knock-out mice generated larger lesions upon carotid ligation and smaller lesions after femoral denudation (Keul et al. 2011, Shimizu et al. 2012). This apparent paradox might be explained by opposing roles of S1PR3 in medial and adventitial cells and depending on the injury model, one or the other might be prevailing.

4.7 Effects of abdominal aortic injury on the proximal aorta

Following clamping of the abdominal aorta, we also harvested the aortic arch and the descending thoracic aorta to investigate possible changes in gene expression. Surgeries were associated with increased medial expression of Myh11 in both proximal aortic regions (Figure 15). One possible reason for this may be the increased blood pressure inflicted on the proximal aorta during clamping of the abdominal aorta. Forces onto the vessel wall generated by blood pressure increases have been shown to activate PI3K/AKT, NF-kB, Rho family GTPases and MAPKs (Haga et al. 2007) and may also include increased Myh11 expression. In addition, upon clamping of the abdominal aorta, we also found increased CD68 expression the aortic region adjunct to the injured stretch. In the more distant aortic arch, only a trend of higher CD68 expression was observed. These observations show that the inflammatory response is not restricted to the injured area but also affects uninjured, adjunct parts of the aorta.

5. Summary and conclusions

This study established that aortic clamping is a suitable mouse model to study IH. Given the larger size of the aorta compared to carotid or femoral arteries, this model allows easy separation of the I-M and the adventitia and generates sufficient material for standard gene expression experiments. Neointimal lesions were observed at 28 days after clamping. The immunofluorescent staining of CD31 shows an early re-endothelialization at 4 days. The cell marker expression measurements and medial cell counts may suggest injury-induced cell apoptosis and adventitial inflammation. Taken together, possible triggers for injury-induced IH involves endothelial denudation, VSMC apoptosis and adventitial inflammation.

Given the injury-induced changes of S1P receptor expression, we assume that S1P plays an important role in response of adventitial cells to arterial injury. Increased S1PR1 and S1PR3 as well as decreased expression of S1PR2 in the adventitia, all indicate increased potential of adventitial cells to proliferate and migrate. S1P may be critical for IH in two ways, as an activator of adventitial cells and also as a chemoattractant of arterial cell to migrate towards lumen. These findings support the idea that the adventitia plays a critical role in regulating IH and that blockade of S1P-S1PR1/S1PR3 signaling might be a promising pharmaceutical target to prevent restenosis in humans.

Zusammenfassung

In Rahmen dieser Arbeit wurde ein experimentelles Modell der Intimahyperplasie durch Klemmen der Aorta in der Maus implementiert und untersucht. Da die Aorta im Vergleich zu Karotiden bzw. Femoralarterien ein deutlich größeres Gefäß darstellt, kann hier die Intima-Media einfach von der Adventitia getrennt werden und auch genügend Material gewonnen werden, um nachfolgend Genexpressionsmessungen mit qPCR durchzuführen. Neointimale Läsionen wurden 28 Tage nach Klemmen der Aorta gefunden. Mittels Immunofluoreszenzfärbungen von CD31 konnte zunächst eine Denudierung und anschließend eine frühe Reendothelialisierung nach nur 4 Tagen gezeigt werden. Die Bestimmungen der medialen Zellzahlen deuten auf eine Apoptose in der Media und Zellmarker für Immunzellen in der Adventitia auf eine Entzündungsreaktion der Adventita hin. All diese Veränderungen können ursächlich für die Intimahyperplasie sein.

Neben diesen Veränderungen war auch die Expression von Sphingosin-1-Phospaht (S1P) Rezeptoren (S1PR) in dem untersuchten Verletzungsmodell insbesondere in der Adventitia verändert. Sowohl eine gesteigerte Expression des S1PR1 und des S1PR3 sowie auch eine verringerte Expression des S1PR2 deuten auf eine gesteigerte Proliferations- und Migrationsfähigkeit dieser Zellen hin. S1P könnte damit die Intimahyperplasie zweifach regulieren, zum einen mittels einer Aktivierung von Adventitiazellen und zum anderen in seiner Funktion als Botenstoff für mediale Zellen, der zu einer verstärkten Migration dieser Zellen in Richtung Lumen führt.

Zusammenfassend lässt sich sagen, dass unsere Beobachtungen die Hypothese unterstützt, dass die Adventitia bei der Regulation der Intimahyperplasie eine entscheidende Rolle spielt und dass eine Blockade der S1P-S1PR1/S1PR3 Signaltransduktion einen vielversprechenden Ansatz darstellen könnte, um eine Restenose nach Gefäßoperationen im Menschen zu verhindern.

6. Abbreviations

ApoM	Apolipoprotein M
BrdU	Bromodesoxyuridine
CD31	Cluster of differentiation 31
CD45	Cluster of differentiation 45
CD68	Cluster of differentiation 68
Cdc42	Cell division control protein 42 homolog
cDNA	complementary deoxyribonucleic acid
CT	Cycle threshold
DAPI	4′,6-Diamidin-2-phenylindol
DES	Drug eluting stents
DNA	Deoxyribonucleic acid
ECs	Endothelial cells
EEL	External elastic lamina
Elk-1	ETS Like protein-1
eNOS	Endothelial nitric oxide synthase
ERK-1/2	Extracellular signal-regulated kinases-1/2
ETS	Erythroblast Transformation Specific
EvG	Elastic van Gieson
GAPDH	Glycerinaldehyd-3-phosphat-dehydrogenase
GFP	Green fluorescent protein
HCASMC	Human coronary artery smooth muscle cell
HDL	High density lipoprotein
H&E	Hematoxylin and eosin
IAA	Infrarenal abdominal aorta
IEL	Internal elastic lamina
IH	Intimal hyperplasia
I-M	Intima-media
IMA	Internal mammary artery
IP3	inositol (1,4,5)-trisphosphate
LPP	Lipid phosphate phosphatases
MFSD2B	Major facilitator superfamily domain- containing protein 2B

MMPs	Matrix metalloproteinases
MRTF	Myocardin-related transcription factor
MYH11	Myosin heavy chain 11
MyD88	Myeloid differentiation protein-88
NF-κB	Nuclear factor 'kappa-light-chain-enhancer' of activated B-cells
NO	Nitric oxide
PCI	Percutaneous coronary intervention
PI3K	Phosphoinositid-3-kinase
PLC	Phospholipase C
PTA	Percutaneous transluminal angioplasty
PTEN	Phosphatase and Tensin homolog
RBCs	Red blood cells
RNA	Ribonucleic acid
siRNA	Small interfering RNA
ROCK	Rho kinase
RT-qPCR	Real time quantitative polymerase chain reaction
S1P	Sphingosine-1-phosphate
S1PRs	Sphingosine-1-phosphate receptors
SGPL	Sphingosine-1-phosphate lyase
SMA	Smooth muscle α-actin
SMC	Smooth muscle cell
SphK	Sphingosine-kinase
SPNS2	Sphingolipid Transporter 2
SPP	S1P phosphatase
SRF	Serum response factor
TCF	Ternary complex factor
VSMC	Vascular smooth muscle cell
YFP	Yellow fluorescent protein

7. References

Abarbanell AM, Herrmann JL, Weil BR, Wang Y, Tan J, Moberly SP, et al. Animal models of myocardial and vascular injury. J Surg Res. 2010;162(2):239-49.

Alewijnse AE, Peters SL, Michel MC. Cardiovascular effects of sphingosine-1-phosphate and other sphingomyelin metabolites. Br J Pharmacol. 2004;143(6):666-84.

Ambler GK, Twine CP. Graft type for femoro-popliteal bypass surgery. The Cochrane database of systematic reviews. 2018;2(2): Cd001487.

Aoki J, Tanabe K. Mechanisms of drug-eluting stent restenosis. Cardiovasc Interv Ther. 2021;36(1):23-9.

Aslanidou L, Trachet B, Reymond P, Fraga-Silva RA, Segers P, Stergiopulos N. A 1D model of the arterial circulation in mice. Altex. 2016;33(1):13-28.

Awojoodu AO, Ogle ME, Sefcik LS, Bowers DT, Martin K, Brayman KL, et al. Sphingosine 1-phosphate receptor 3 regulates recruitment of anti-inflammatory monocytes to microvessels during implant arteriogenesis. Proc Natl Acad Sci U S A. 2013;110(34):13785-90.

Barton M, Grüntzig J, Husmann M, Rösch J. Balloon Angioplasty - The Legacy of Andreas Grüntzig, M.D. (1939-1985). Front Cardiovasc Med. 2014; 1:15.

Bath PM, Hassall DG, Gladwin AM, Palmer RM, Martin JF. Nitric oxide and prostacyclin. Divergence of inhibitory effects on monocyte chemotaxis and adhesion to endothelium in vitro. Arterioscler Thromb. 1991;11(2):254-60.

Becquemin JP, Favre JP, Marzelle J, Nemoz C, Corsin C, Leizorovicz A. Systematic versus selective stent placement after superficial femoral artery balloon angioplasty: a multicenter prospective randomized study. J Vasc Surg. 2003;37(3):487-94.

Bennett MR. Apoptosis of vascular smooth muscle cells in vascular remodelling and atherosclerotic plaque rupture. Cardiovasc Res 1999;41(2):361-8.

Bittl JA, Chew DP, Topol EJ, Kong DF, Califf RM. Meta-analysis of randomized trials of percutaneous transluminal coronary angioplasty versus atherectomy, cutting balloon atherotomy, or laser angioplasty. J Am Coll Cardiol. 2004;43(6):936-42.

Braetz J, Becker A, Geissen M, Larena-Avellaneda A, Schrepfer S, Daum G. Sphingosine-1-phosphate receptor 1 regulates neointimal growth in a humanized model for restenosis. J Vasc Surg. 2018;68:201-7.

Buccheri D, Piraino D, Andolina G, Cortese B. Understanding and managing in-stent restenosis: a review of clinical data, from pathogenesis to treatment. J Thorac Dis. 2016;8(10): E1150-E62.

Chen L, DeWispelaere A, Dastvan F, Osborne WR, Blechner C, Windhorst S, et al.

Smooth Muscle-Alpha Actin Inhibits Vascular Smooth Muscle Cell Proliferation and Migration by Inhibiting Rac1 Activity. PLoS One. 2016;11(5):e0155726.

Chen Y, Wong MM, Campagnolo P, Simpson R, Winkler B, Margariti A, et al. Adventitial stem cells in vein grafts display multilineage potential that contributes to neointimal formation. Arterioscler Thromb Vasc Biol. 2013;33(8):1844-51.

Christoffersen C, Obinata H, Kumaraswamy S, Galvani S, Ahnstrom J, Sevvana M, et al. Endothelium-protective sphingosine-1-phosphate provided by HDL-associated apolipoprotein M. Proc Natl Acad Sci USA. 2011; 108:9613 - 8.

Clowes AW, Reidy MA, Clowes MM. Kinetics of cellular proliferation after arterial injury. I. Smooth muscle growth in the absence of endothelium. Lab Invest 1983;49(3):327-33.

Colombo A, Drzewiecki J, Banning A, Grube E, Hauptmann K, Silber S, et al. Randomized study to assess the effectiveness of slow- and moderate-release polymer-based paclitaxel-eluting stents for coronary artery lesions. Circulation. 2003;108(7):788-94.

Das M, Bouchey DM, Moore MJ, Hopkins DC, Nemenoff RA, Stenmark KR. Hypoxia-induced proliferative response of vascular adventitial fibroblasts is dependent on g protein-mediated activation of mitogen-activated protein kinases. J Biol Chem. 2001;276(19):15631-40.

Dormandy JA, Rutherford RB. Management of peripheral arterial disease (PAD). TASC Working Group. TransAtlantic Inter-Society Consensus (TASC). J Vasc Surg. 2000;31(1 Pt 2): S1-s296.

Dörr F. H.-H. Perkampus: UV-VIS-Spektroskopie und ihre Anwendungen, Springer-Verlag, Berlin, Heidelberg, New York, Tokyo 1986. 208 Seiten, 75 Abb., 21 Tab. VIII, gebunden DM 148,—. Berichte der Bunsengesellschaft für physikalische Chemie. 1986;90(10):922-.

Dutzmann J, Koch A, Weisheit S, Sonnenschein K, Korte L, Haertle M, et al. Sonic hedgehog-dependent activation of adventitial fibroblasts promotes neointima formation. Cardiovasc Res. 2017;113(13):1653-63.

Fukata Y, Amano M, Kaibuchi K. Rho-Rho-kinase pathway in smooth muscle contraction and cytoskeletal reorganization of non-muscle cells. Trends Pharmacol Sci. 2001;22(1):32-9.

Fukuhara S, Simmons S, Kawamura S, Inoue A, Orba Y, Tokudome T, et al. The sphingosine-1-phosphate transporter Spns2 expressed on endothelial cells regulates lymphocyte trafficking in mice. J Clin Invest. 2012;122(4):1416-26.

Galkina E, Kadl A, Sanders J, Varughese D, Sarembock IJ, Ley K. Lymphocyte recruitment into the aortic wall before and during development of atherosclerosis is partially L-selectin dependent. J Exp Med. 2006;203(5):1273-82.

Gallagher SR, Desjardins PR. Quantitation of DNA and RNA with Absorption and Fluorescence Spectroscopy. Curr Protoc Mol Biol. 2006;76(1):A.3D.1-A.3D.21.

Galvani S, Sanson M, Blaho VA, Swendeman SL, Conger H, Dahlbäck B, et al. HDL-bound sphingosine 1-phosphate acts as a biased agonist for the endothelial cell receptor S1P1 to limit vascular inflammation. Science signaling. 2015;8(389):ra79-ra.

Goparaju SK, Jolly PS, Watterson KR, Bektas M, Alvarez S, Sarkar S, et al. The S1P2 receptor negatively regulates platelet-derived growth factor-induced motility and proliferation. Mol Cell Biol. 2005;25(10):4237-49.

Grabski AD, Shimizu T, Deou J, Mahoney WM, Jr., Reidy MA, Daum G. Sphingosine-1-Phosphate Receptor-2 Regulates Expression of Smooth Muscle Alpha-Actin After Arterial Injury. Arterioscler Thromb Vasc Biol. 2009;29(10):1644-50.

Grudzinska MK, Kurzejamska E, Hagemann N, Bojakowski K, Soin J, Lehmann MH, et al. Monocyte chemoattractant protein 1-mediated migration of mesenchymal stem cells is a source of intimal hyperplasia. Arterioscler Thromb Vasc Biol. 2013;33(6):1271-9.

Haga JH, Li YS, Chien S. Molecular basis of the effects of mechanical stretch on vascular smooth muscle cells. J Biomech. 2007;40(5):947-60.

Havelka GE, Kibbe MR. The vascular adventitia: its role in the arterial injury response. Vasc Endovascular Surg. 2011;45(5):381-90.

Hayashi K, Nakamura S, Morishita R, Moriguchi A, Aoki M, Matsumoto K, et al. In vivo transfer of human hepatocyte growth factor gene accelerates re-endothelialization and inhibits neointimal formation after balloon injury in rat model. Gene Ther. 2000;7(19):1664-71.

Holmes DR, Jr., Vlietstra RE, Smith HC, Vetrovec GW, Kent KM, Cowley MJ, et al. Restenosis after percutaneous transluminal coronary angioplasty (PTCA): a report from the PTCA Registry of the National Heart, Lung, and Blood Institute. Am J Cardiol. 1984;53(12):77c-81c.

Hui DY. Intimal hyperplasia in murine models. Curr Drug Targets. 2008;9(3):251-60.

Ikeda H, Satoh H, Yanase M, Inoue Y, Tomiya T, Arai M, et al. Antiproliferative property of sphingosine 1-phosphate in rat hepatocytes involves activation of Rho via Edg-5. Gastroenterology. 2003;124(2):459-69.

Illuminati G, Belmonte R, Schneider F, Pizzardi G, Calio FG, Ricco JB. Prosthetic bypass for restenosis after endarterectomy or stenting of the carotid artery. J Vasc Surg. 2017;65(6):1664-72.

Inoue S, Nakazawa T, Cho A, Davastan F, Shilling D, Daum G, et al. Regulation of arterial lesions in mice depends on differential smooth muscle cell migration: A role for sphingosine-1-phosphate receptors. J Vasc Surg. 2007;46(4):756-63.

Jennette JC, Stone JR. Chapter 11 - Diseases of Medium-Sized and Small Vessels. In: Willis MS, Homeister JW, Stone JR, editors. Cellular and Molecular Pathobiology of Cardiovascular Disease. San Diego: Academic Press; 2014. p. 197-219.

Katras T, Baltazar U, Rush DS, Sutterfield WC, Harvill LM, Stanton PE, Jr. Durability of eversion carotid endarterectomy: comparison with primary closure and carotid patch angioplasty. J Vasc Surg. 2001;34(3):453-8.

Keller CD, Rivera Gil P, Tolle M, van der Giet M, Chun J, Radeke HH, et al. Immunomodulator FTY720 Induces Myofibroblast Differentiation via the Lysophospholipid Receptor S1P3 and Smad3 Signaling. Am J Pathol. 2007;170(1):281-92.

Keul P, Lucke S, von Wnuck Lipinski K, Bode C, Graler M, Heusch G, et al. Sphingosine-1-Phosphate Receptor 3 Promotes Recruitment of Monocyte/Macrophages in Inflammation and Atherosclerosis. Circ Res. 2011;108(3):314-23.

Kohler TR, Toleikis PM, Gravett DM, Avelar RL. Inhibition of neointimal hyperplasia in a sheep model of dialysis access failure with the bioabsorbable Vascular Wrap paclitaxel-eluting mesh. J Vasc Surg. 2007;45(5):1029-37; discussion 37-8.

Kraiss L, Clowes AJTbsovd. Response of the arterial wall to injury and intimal hyperplasia. 1997:289-317.

Lal BK, Hobson RW, 2nd, Goldstein J, Geohagan M, Chakhtoura E, Pappas PJ, et al. In-stent recurrent stenosis after carotid artery stenting: life table analysis and clinical relevance. J Vasc Surg. 2003;38(6):1162-8; discussion 9.

Lee MJ, Thangada S, Claffey KP, Ancellin N, Liu CH, Kluk M, et al. Vascular endothelial cell adherens junction assembly and morphogenesis induced by sphingosine-1-phosphate. Cell. 1999;99(3):301-12.

Leertouwer TC, Gussenhoven EJ, Bosch JL, van Jaarsveld BC, van Dijk LC, Deinum J, et al. Stent placement for renal arterial stenosis: where do we stand? A meta-analysis. Radiology. 2000;216(1):78-85.

Lemson MS, Tordoir JH, Daemen MJ, Kitslaar PJ. Intimal hyperplasia in vascular grafts. Eur J Vasc Endovasc Surg. 2000;19(4):336-50.

Li G, Chen S-J, Oparil S, Chen Y-F, Thompson JA. Direct In Vivo Evidence Demonstrating Neointimal Migration of Adventitial Fibroblasts After Balloon Injury of Rat Carotid Arteries. Circulation. 2000;101(12):1362-5.

Liu Y, Wada R, Yamashita T, Mi Y, Deng CX, Hobson JP, et al. Edg-1, the G protein-coupled receptor for sphingosine-1-phosphate, is essential for vascular maturation. J Clin Invest. 2000;106(8):951-61.

Livak KJ, Schmittgen TD. Analysis of relative gene expression data using real-time quantitative PCR and the 2(-Delta Delta C(T)) Method. Methods. 2001;25(4):402-8.

Lockman K, Hinson JS, Medlin MD, Morris D, Taylor JM, Mack CP. Sphingosine 1-phosphate stimulates smooth muscle cell differentiation and proliferation by activating separate serum response factor co-factors. J Biol Chem. 2004;279(41):42422-30.

Lorenz JN, Arend LJ, Robitz R, Paul RJ, MacLennan AJ. Vascular dysfunction in S1P2 sphingosine 1-phosphate receptor knockout mice. Am J Physiol Regul Integr Comp Physiol. 2007;292(1):R440-6. Epub 2006 Sep 21.

Mack CP, Somlyo AV, Hautmann M, Somlyo AP, Owens GK. Smooth muscle differentiation marker gene expression is regulated by RhoA-mediated actin polymerization. J Biol Chem. 2001;276(1):341-7.

Majesky MW. Vascular Smooth Muscle Cells. Arterioscler Thromb Vasc Biol. 2016;36(10): e82-6.

Mattsson EJ, Kohler TR, Vergel SM, Clowes AW. Increased blood flow induces regression of intimal hyperplasia. Arterioscler Thromb Vasc Biol 1997;17(10):2245-9.

McDonald OG, Wamhoff BR, Hoofnagle MH, Owens GK. Control of SRF binding to CArG box chromatin regulates smooth muscle gene expression in vivo. J Clin Invest. 2006;116(1):36-48.

Mendelson K, Evans T, Hla T. Sphingosine 1-phosphate signalling. Development. 2014;141(1):5-9.

Michaud J, Im D-S, Hla T. Inhibitory Role of Sphingosine 1-Phosphate Receptor 2 in Macrophage Recruitment during Inflammation. J Immunol. 2010;184(3):1475-83.

Mills B, Robb T, Larson DF. Intimal hyperplasia: slow but deadly. Perfusion. 2012;27(6):520-8.

Miura Y, Kanamaru H, Yasuda R, Toma N, Suzuki H. Nonfasting Triglyceride as an Independent Predictor of Carotid Restenosis After Carotid Endarterectomy or Carotid Artery Stenting. World Neurosurg. 2021.

Miwa K, Asano M, Horai R, Iwakura Y, Nagata S, Suda T. Caspase 1-independent IL-1beta release and inflammation induced by the apoptosis inducer Fas ligand. Nat Med. 1998;4(11):1287-92.

Morales-Ruiz M, Lee MJ, Zöllner S, Gratton JP, Scotland R, Shiojima I, et al. Sphingosine 1-phosphate activates Akt, nitric oxide production, and chemotaxis through a Gi protein/phosphoinositide 3-kinase pathway in endothelial cells. J Biol Chem. 2001;276(22):19672-7.

Moses JW, Leon MB, Popma JJ, Fitzgerald PJ, Holmes DR, O'Shaughnessy C, et al. Sirolimus-eluting stents versus standard stents in patients with stenosis in a native coronary artery. N Engl J Med. 2003;349(14):1315-23.

Murakami A, Takasugi H, Ohnuma S, Koide Y, Sakurai A, Takeda S, et al. Sphingosine 1-phosphate (S1P) regulates vascular contraction via S1P3 receptor: investigation based on a new S1P3 receptor antagonist. Mol Pharmacol. 2010;77(4):704-13.

Nemenoff RA, Horita H, Ostriker AC, Furgeson SB, Simpson PA, VanPutten V, et al. SDF-1α induction in mature smooth muscle cells by inactivation of PTEN is a

critical mediator of exacerbated injury-induced neointima formation. Arterioscler Thromb Vasc Biol. 2011;31(6):1300-8.

Newman AA, Baylis RA, Hess DL, Griffith SD, Shankman LS, Cherepanova OA, et al. Irradiation abolishes smooth muscle investment into vascular lesions in specific vascular beds. JCI insight. 2018;3(15).

Nincheri P, Luciani P, Squecco R, Donati C, Bernacchioni C, Borgognoni L, et al. Sphingosine 1-phosphate induces differentiation of adipose tissue-derived mesenchymal stem cells towards smooth muscle cells. Cell Mol Life Sci. 2009;66(10):1741-54.

Nofer JR, van der Giet M, Tolle M, Wolinska I, von Wnuck Lipinski K, Baba HA, et al. HDL induces NO-dependent vasorelaxation via the lysophospholipid receptor S1P3. J Clin Invest. 2004;113(4):569-81.

Nomoto A, Mutoh S, Hagihara H, Yamaguchi I. Smooth muscle cell migration induced by inflammatory cell products and its inhibition by a potent calcium antagonist, nilvadipine. Atherosclerosis. 1988;72(2-3):213-9.

Nussbaum C, Bannenberg S, Keul P, Gräler MH, Gonçalves-de-Albuquerque CF, Korhonen H, et al. Sphingosine-1-phosphate receptor 3 promotes leukocyte rolling by mobilizing endothelial P-selectin. Nature communications. 2015;6.

Okamoto H, Takuwa N, Yokomizo T, Sugimoto N, Sakurada S, Shigematsu H, et al. Inhibitory regulation of Rac activation, membrane ruffling, and cell migration by the G protein-coupled sphingosine-1-phosphate receptor EDG5 but not EDG1 or EDG3. Mol Cell Biol. 2000;20(24):9247-61.

Ouyang J, Shu Z, Chen S, Xiang H, Lu H. The role of sphingosine 1-phosphate and its receptors in cardiovascular diseases. J Cell Mol Med. 2020;24(18):10290-301.

Owens GK, Kumar MS, Wamhoff BR. Molecular regulation of vascular smooth muscle cell differentiation in development and disease. Physiol Rev. 2004;84(3):767-801.

Patel SD, Waltham M, Wadoodi A, Burnand KG, Smith A. The role of endothelial cells and their progenitors in intimal hyperplasia. Ther Adv Cardiovasc Dis. 2010;4(2):129-41.

Puel J, Juilliere Y, Bertrand ME, Rickards AF, Sigwart U, Serruys PW. Early and late assessment of stenosis geometry after coronary arterial stenting. Am J Cardiol. 1988;61(8):546-53.

Remy-Martin JP, Marandin A, Challier B, Bernard G, Deschaseaux M, Herve P, et al. Vascular smooth muscle differentiation of murine stroma: a sequential model. Exp Hematol. 1999;27(12):1782-95.

Rensen SSM, Doevendans PAFM, van Eys GJJM. Regulation and characteristics of vascular smooth muscle cell phenotypic diversity. Netherlands heart journal : monthly journal of the Netherlands Society of Cardiology and the Netherlands Heart Foundation. 2007;15(3):100-8.

Ridley AJ. Rho GTPase signalling in cell migration. Curr Opin Cell Biol. 2015; 36:103-12.

Ryu Y, Takuwa N, Sugimoto N, Sakurada S, Usui S, Okamoto H, et al. Sphingosine-1-phosphate, a platelet-derived lysophospholipid mediator, negatively regulates cellular Rac activity and cell migration in vascular smooth muscle cells. Circ Res. 2002;90(3):325-32.

Sanchez T. Sphingosine-1-Phosphate Signaling in Endothelial Disorders. Current Atherosclerosis Reports. 2016;18(6):1-13.

Sartore S, Chiavegato A, Faggin E, Franch R, Puato M, Ausoni S, et al. Contribution of Adventitial Fibroblasts to Neointima Formation and Vascular Remodeling: From Innocent Bystander to Active Participant. Circ Res. 2001;89(12):1111-21.

Sata M, Maejima Y, Adachi F, Fukino K, Saiura A, Sugiura S, et al. A mouse model of vascular injury that induces rapid onset of medial cell apoptosis followed by reproducible neointimal hyperplasia. J Mol Cell Cardiol. 2000;32(11):2097-104.

Sata M, Saiura A, Kunisato A, Tojo A, Okada S, Tokuhisa T, et al. Hematopoietic stem cells differentiate into vascular cells that participate in the pathogenesis of atherosclerosis. Nat Med. 2002;8(4):403-9.

Schwartz SM, Stemerman MB, Benditt EP. The aortic intima. II. Repair of the aortic lining after mechanical denudation. Am J Pathol. 1975;81(1):15-42.

Shi Y, O'Brien JE, Fard A, Mannion JD, Wang D, Zalewski A. Adventitial Myofibroblasts Contribute to Neointimal Formation in Injured Porcine Coronary Arteries. Circulation. 1996;94(7):1655-64.

Shimizu T, De Wispelaere A, Winkler M, D'Souza T, Caylor J, Chen L, et al. Sphingosine-1-Phosphate Receptor 3 Promotes Neointimal Hyperplasia in Mouse Iliac-Femoral Arteries. Arterioscler Thromb Vasc Biol. 2012;32(4):955-61.

Shimizu T, Nakazawa T, Cho A, Dastvan F, Shilling D, Daum G, et al. Sphingosine 1-Phosphate Receptor 2 Negatively Regulates Neointimal Formation in Mouse Arteries. Circ Res. 2007;101:995-1000.

Shimokawa H, Ito A, Fukumoto Y, Kadokami T, Nakaike R, Sakata M, et al. Chronic treatment with interleukin-1 beta induces coronary intimal lesions and vasospastic responses in pigs in vivo. The role of platelet-derived growth factor. J Clin Invest. 1996;97(3):769-76.

Shirali AS, McDonald AI, Mack JJ, Iruela-Arispe ML. Reproducible Arterial Denudation Injury by Infrarenal Abdominal Aortic Clamping in a Murine Model. Journal of visualized experiments: JoVE. 2016(117).

Simper D, Stalboerger PG, Panetta CJ, Wang S, Caplice NM. Smooth muscle progenitor cells in human blood. Circulation. 2002;106(10):1199-204.

Siow RCM, Mallawaarachchi CM, Weissberg PL. Migration of adventitial myofibroblasts following vascular balloon injury: insights from in vivo gene transfer to rat carotid

arteries. Cardiovasc Res. 2003;59(1):212-21.

Stenmark KR, Yeager ME, El Kasmi KC, Nozik-Grayck E, Gerasimovskaya EV, Li M, et al. The adventitia: essential regulator of vascular wall structure and function. Annu Rev Physiol. 2013; 75:23-47.

Stoney RJ, String ST. Recurrent carotid stenosis. Surgery. 1976;80(6):705-10.

Taha TA, Argraves KM, Obeid LM. Sphingosine-1-phosphate receptors: receptor specificity versus functional redundancy. Biochim Biophys Acta. 2004;1682(1-3):48-55.

Tanaka K, Sata M, Hirata Y, Nagai R. Diverse contribution of bone marrow cells to neointimal hyperplasia after mechanical vascular injuries. Circ Res. 2003;93(8):783-90. Epub 2003 Sep 18.

Tang PC, Qin L, Zielonka J, Zhou J, Matte-Martone C, Bergaya S, et al. MyD88-dependent, superoxide-initiated inflammation is necessary for flow-mediated inward remodeling of conduit arteries. J Exp Med. 2008;205(13):3159-71.

Tölle M, Klöckl L, Wiedon A, Zidek W, van der Giet M, Schuchardt M. Regulation of endothelial nitric oxide synthase activation in endothelial cells by S1P1 and S1P3. Biochem Biophys Res Commun. 2016;476(4):627-34.

Tseng H, Peterson TE, Berk BC. Fluid shear stress stimulates mitogen-activated protein kinase in endothelial cells. Circ Res 1995;77(5):869-78.

Vu TM, Ishizu AN, Foo JC, Toh XR, Zhang F, Whee DM, et al. Mfsd2b is essential for the sphingosine-1-phosphate export in erythrocytes and platelets. Nature. 2017;550(7677):524-8.

Walsh K, Smith RC, Kim HS. Vascular cell apoptosis in remodeling, restenosis, and plaque rupture. Circ Res. 2000;87(3):184-8.

Wamhoff BR, Lynch KR, Macdonald TL, Owens GK. Sphingosine-1-Phosphate Receptor Subtypes Differentially Regulate Smooth Muscle Cell Phenotype. Arterioscler Thromb Vasc Biol. 2008;28(8):1454-61.

Wang Z, Wang DZ, Hockemeyer D, McAnally J, Nordheim A, Olson EN. Myocardin and ternary complex factors compete for SRF to control smooth muscle gene expression. Nature. 2004;428(6979):185-9.

Weintraub WS. The Pathophysiology and Burden of Restenosis. The American Journal of Cardiology. 2007;100(5, Supplement 1): S3-S9.

Welt FG, Rogers C. Inflammation and restenosis in the stent era. Arterioscler Thromb Vasc Biol. 2002;22(11):1769-76.

Wilcox JN, Scott NA. Potential role of the adventitia in arteritis and atherosclerosis. Int J Cardiol. 1996;54 Suppl: S21-35.

Winkler MS, Nierhaus A, Poppe A, Greiwe G, Graler MH, Daum G. Sphingosine-1-

Phosphate: A Potential Biomarker and Therapeutic Target for Endothelial Dysfunction and Sepsis? Shock. 2017;47(6):666-72.

Xiong Y, Hla T. S1P control of endothelial integrity. Curr Top Microbiol Immunol. 2014;378:85-105.

Xu Q, Zhang Z, Davison F, Hu Y. Circulating progenitor cells regenerate endothelium of vein graft atherosclerosis, which is diminished in ApoE-deficient mice. Circ Res. 2003;93(8): e76-86.

Xu QB. Endothelial progenitor cells in angiogenesis. Sheng Li Xue Bao. 2005;57(1):1-6.

Zhang G, Yang L, Kim GS, Ryan K, Lu S, O'Donnell RK, et al. Critical role of sphingosine-1-phosphate receptor 2 (S1PR2) in acute vascular inflammation. Blood. 2013;122(3):443-55.

Zhang J-M, Wang Y, Miao Y-J, Zhang Y, Wu Y-N, Jia L-X, et al. Knockout of CD8 Delays Reendothelialization and Accelerates Neointima Formation in Injured Arteries of Mouse via TNF-α Inhibiting the Endothelial Cells Migration. PLoS One. 2013;8(5):e62001.

8. Acknowledgement

9. Curriculum Vitae

Personal Information

Name: Yu Jiang

Date of Birth: 19.12.1991

Place of Birth: Jiangsu

Education

2017 – : MD study at Universität Hamburg

2015 – 2017: Master of Clinical Medicine, Southeast University, Nanjing, PR of China

2010 – 2015: Bachelor of Clinical Medicine, Southeast University, Nanjing, PR of China

2007 – 2010: Qianhuang High School, Changzhou, PR of China

1998 – 2007: Wujin Star Experimental School, Changzhou, PR of China

Internship

2015 – 2017: Nanjing Drum Tower Hospital, the Affiliated Hospital of Nanjing University Medical School, Nanjing, PR of China

2015 – 2016: Jiangsu Key Laboratory of Molecular Medicine, Medical School of Nanjing University, Nanjing, PR of China

2014 – 2015: Nanjing Drum Tower Hospital, the Affiliated Hospital of Nanjing University Medical School, Nanjing, PR of China

Publications

Hao S, Song C, Shang L, Yu J, Qiao T, Li K. Phosphorylation of Akt by SC79 Prevents Iron Accumulation and Ameliorates Early Brain Injury in a Model of Experimental Subarachnoid Hemorrhage. Molecules. 2016 Mar 10;21(3):325.

Cai J, Jiang Y, Zhang M, Zhao H, Li H, Li K, Zhang X, Qiao T. Protective effects of mitochondrion-targeted peptide SS-31 against hind limb ischemia-reperfusion injury. J Physiol Biochem. 2018 May;74(2):335-343.

Hamburg, 28.11.2021

10. Eidesstattliche Versicherung

Ich versichere ausdrücklich, dass ich die Arbeit selbständig und ohne fremde Hilfe verfasst, andere als die von mir angegebenen Quellen und Hilfsmittel nicht benutzt und die aus den benutzten Werken wörtlich oder inhaltlich entnommenen Stellen einzeln nach Ausgabe (Auflage und Jahr des Erscheinens), Band und Seite des benutzten Werkes kenntlich gemacht habe.

Ferner versichere ich, dass ich die Dissertation bisher nicht einem Fachvertreter an einer anderen Hochschule zur Überprüfung vorgelegt oder mich anderweitig um Zulassung zur Promotion beworben habe.

Ich erkläre mich einverstanden, dass meine Dissertation vom Dekanat der Medizinischen Fakultät mit einer gängigen Software zur Erkennung von Plagiaten überprüft werden kann.

Unterschrift: ....

Yu Jiang